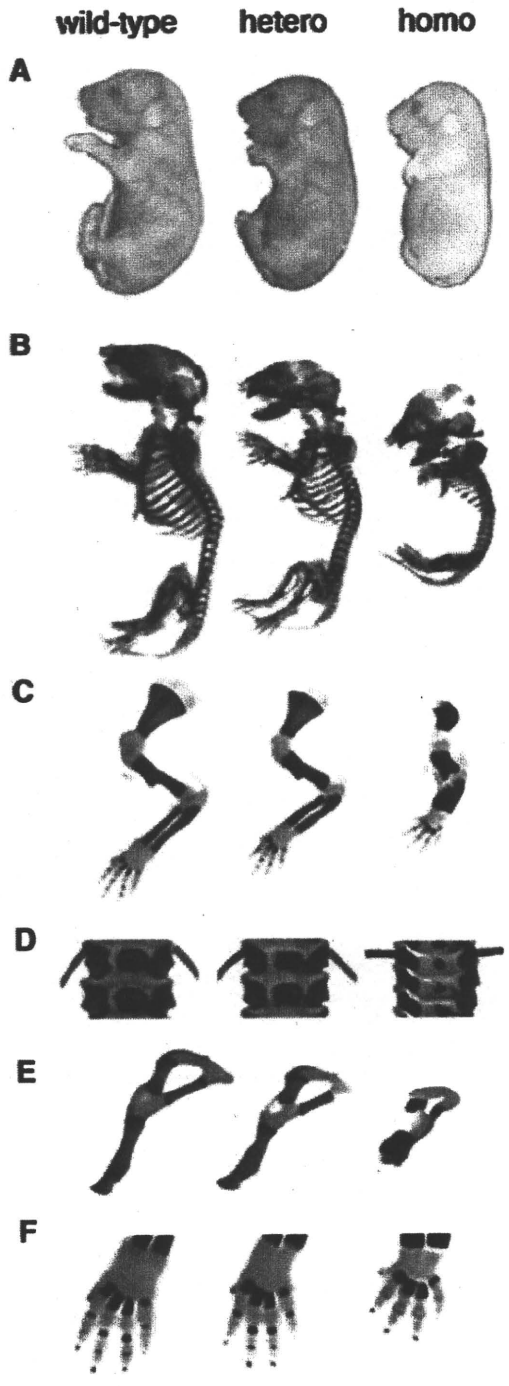

Fig. 2 Gross appearances and skeletal specimens of *Col2a1*^{Rgsc856} mutants at E18.5. **a** Gross appearances. **b–f** Skeletal specimens of whole skeleton (**b**), forelimb (**c**), lumbar spine (**d**), ilia (**e**), and forepaw (**f**). The homozygotes exhibited a severe skeletal dysplasia, including extremely shortened limbs, platyspondyly, severe pelvic hypoplasia, and brachydactyly

growth plate cartilage of *Col2a1*^{Rgsc856} mutants at E19.5 (Fig. 3). The growth plate of wild-type mice is composed of three distinct layers of chondrocytes—resting, proliferating, and hypertrophic zones—representing various stages of differentiation (Fig. 3A). Proliferating chondrocytes were well spaced by extracellular matrix (ECM) and exhibited typical columnar alignment with a flat shape (Fig. 3Ab). In the heterozygotes, this columnar alignment became disordered with reduced ECM spaces (Fig. 3Bb). In the homozygotes, the total length of the growth plate was drastically reduced but the diameter was increased (Fig. 3C). The columnar alignment of proliferating chondrocytes was completely lost (Fig. 3Cb), but hypertrophic chondrocytes were observed (Fig. 3Cc). The shape of the chondrocytes changed to a spindle-like cell in the resting and proliferating zones (Fig. 3Ca, Cb). Staining with toluidine blue, which binds to proteoglycans present in cartilage ECM, showed a drastic reduction in cartilage ECM in the proliferating zone of the homozygotes (Fig. 3D–F).

Characterization of molecular defects in the chondrocytes of *Col2a1*^{Rgsc856} mutants

We investigated the localization of type II collagen in the cartilage of *Col2a1*^{Rgsc856} mutants by immunohistochemical analysis using the sections from the proliferating zone of the femur at E19.5. In wild-type mice and the heterozygotes, immunoreactivity of type II collagen was observed mainly in the extracellular space of chondrocytes (Fig. 4a, b). In contrast, that in the homozygotes was scarcely detected in the extracellular space and was detected mainly in the intracellular space (Fig. 4c). Results of double staining with KDEL, an ER marker, suggested that a part of the mutant type II collagen was accumulating in the ER of chondrocytes in the homozygote (Fig. 4i).

We next performed an electron microscope analysis using samples from the proliferating zone of the femur at E18.5. In wild-type ECM, the collagen fibers showed dense and uniform distribution and many proteoglycan aggregations were found (Fig. 5a). The collagen fibers of the heterozygotes seemed to be slightly less dense (Fig. 5b), and those of the homozygotes were markedly reduced (Fig. 5c). Proteoglycan aggregates were also reduced and irregular in size in the homozygotes. Proliferating chondrocytes in wild-type mice contained well-developed organized rough ER (Fig. 5d). The rough ER was abnormally expanded in both the heterozygotes and the homozygotes (Fig. 5e, f). In the homozygotes, more expanded rough ER was evident compared to the heterozygotes.

Abnormally expanded rough ER and subsequent induction of ER stress have been reported in many mouse lines expressing mutant ECM proteins (Bateman et al. 2009). Expanded rough ER was also observed in mice lacking the ER stress sensor *Bbf2h7* (Saito et al. 2009). Therefore, we measured mRNA levels of two ER stress-related genes,

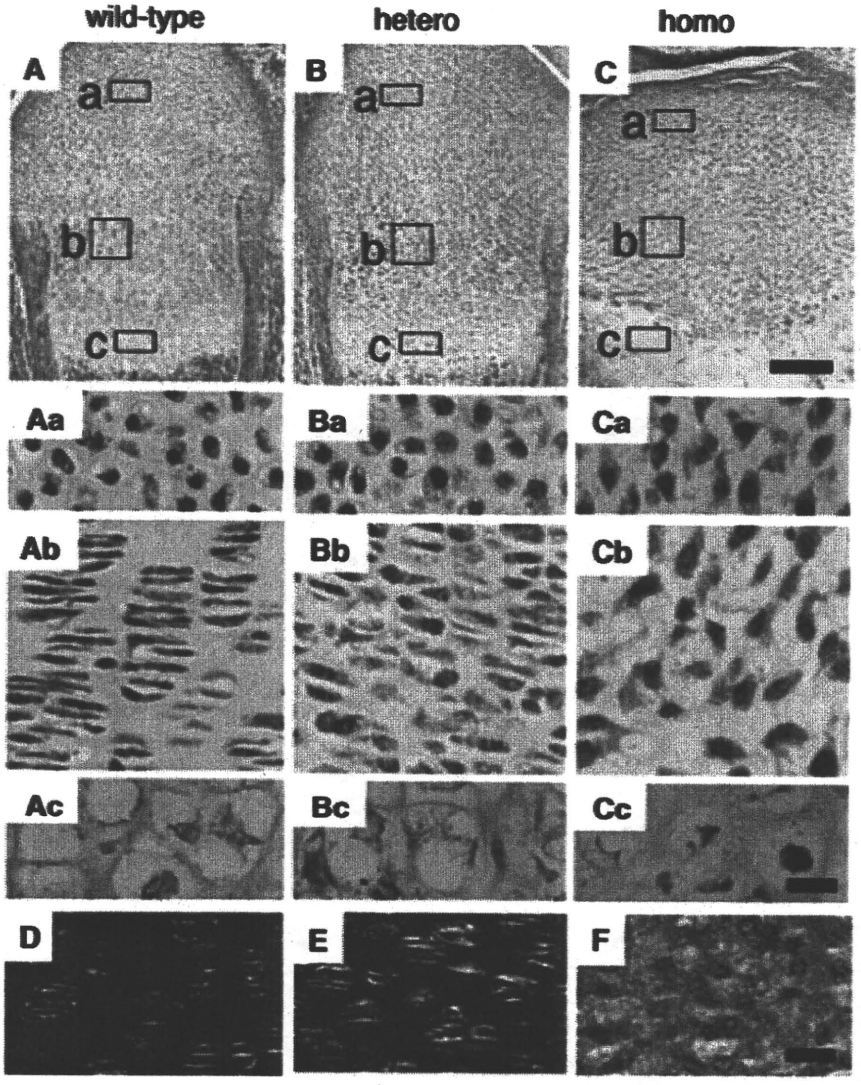

Fig. 3 Histology of growth plate cartilage from *Col2a1*^{Rgsc856} mutants at E19.5. **A–C** Hematoxylin & eosin (HE)–stained sections of the growth plate cartilage. The boxed regions (**a**, **b**, and **c**) represent the resting, proliferating, and hypertrophic zones, respectively. Magnified views of the boxed regions are shown in the same columns. **D–F** Toluidine blue-stained sections of the proliferating zone of the growth plate cartilage. Note that the total length of the growth plate cartilage was drastically reduced in the homozygotes (**C**). The typical columnar alignment of proliferating chondrocytes was observed in wild-type mice (**Ab**) but became disordered in the heterozygotes (**Bb**). This alignment was completely lost in the homozygotes (**Cb**). Weak staining by toluidine blue was evident in the homozygotes (**F**). *Scale bars* 50 μm (**A-C**) and 10 μm (**Aa–Cc** and **D–F**)

Grp94 and *Chop*, using rib cartilage samples at E18.5 (Fig. 6). GRP94 is an ER-resident chaperone, and CHOP is a transcription factor used as an ER stress marker (Bateman et al. 2009). Both genes are reported to be upregulated by ER stress. Their expression levels in both the heterozygotes and the homozygotes were significantly higher than those in wild-type mice, suggesting that ER stress was induced in *Col2a1*^{Rgsc856} mutants.

Osteoarthritis phenotypes in *Col2a1*^{Rgsc856} heterozygotes

Human diseases with *COL2A1* mutations are associated with early-onset OA (Loughlin 2001; Vikkula et al. 1993), and *Dmm* heterozygous mice develop early-onset OA that is conspicuous from 3 through 22 months of age (Bomsta et al. 2006). Therefore, we observed the histological appearance of the knee and elbow joints from wild-type mice and *Col2a1*^{Rgsc856} heterozygotes at 10 months of age. We stained the sections with safranin O (Fig. 7a) and evaluated OA severity with the modified Mankin scoring system (Fig. 7b). In both knee (Fig. 7) and elbow sections (data not shown), there were no significant differences in the score between wild-type and *Col2a1*^{Rgsc856} heterozygotes. In contrast to *Dmm* heterozygotes, *Col2a1*^{Rgsc856} heterozygotes did not show more severe degeneration of articular cartilage than wild-type mice at 10 months of age.

Discussion

Through phenotype-based screening in a large-scale ENU mutagenesis program, we identified a novel *Col2a1* mutant allele—*Col2a1*^{Rgsc856}. The mouse with *Col2a1*^{Rgsc856} is the second mutant with an endogenous C-propeptide mutation in *Col2a1* and the first animal model of PLSD-T. In the

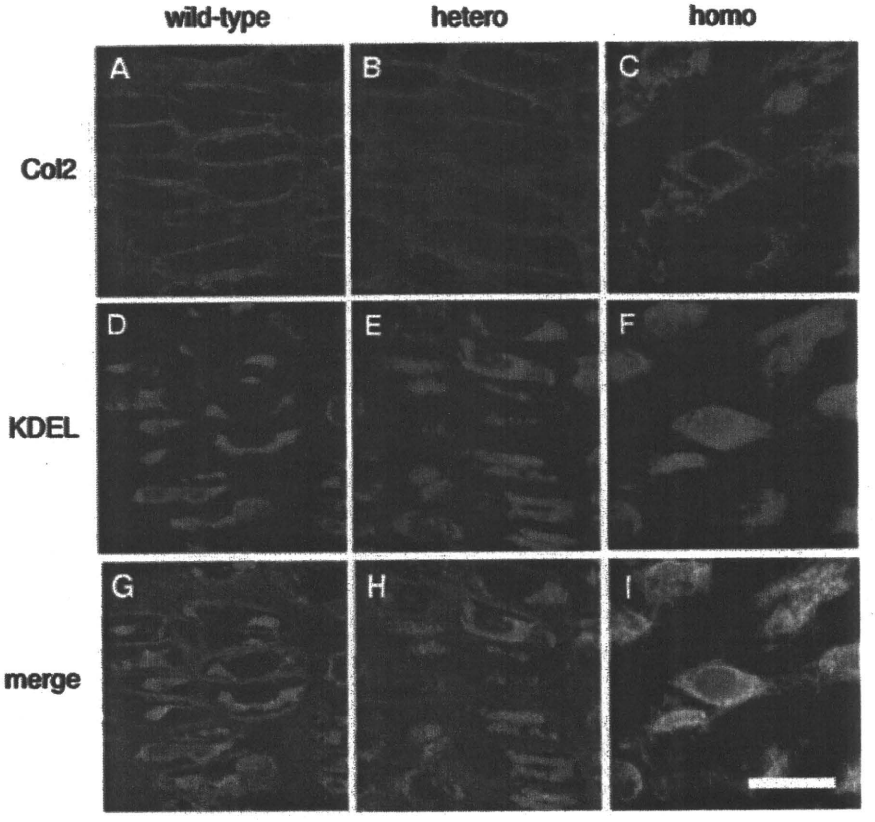

Fig. 4 Immunohistochemistry of type II collagen in the cartilage of *Col2a1*^{Rgsc856} mutants at E19.5. **a–c** The sections of the proliferating zone were stained with a type II collagen antibody. **d–f** Sections were stained with a KDEL (an ER marker) antibody. **g** Merge of **a** and **d**. **h** Merge of **b** and **e**. **i** Merge of **c** and **f**. Note that the immunoreactivity of type II collagen in wild-type mice (**a**) and the heterozygotes (**b**) was observed mainly in the extracellular space. In contrast, that in the homozygotes was in the intracellular space (**c**). *Scale bars* 10 μm

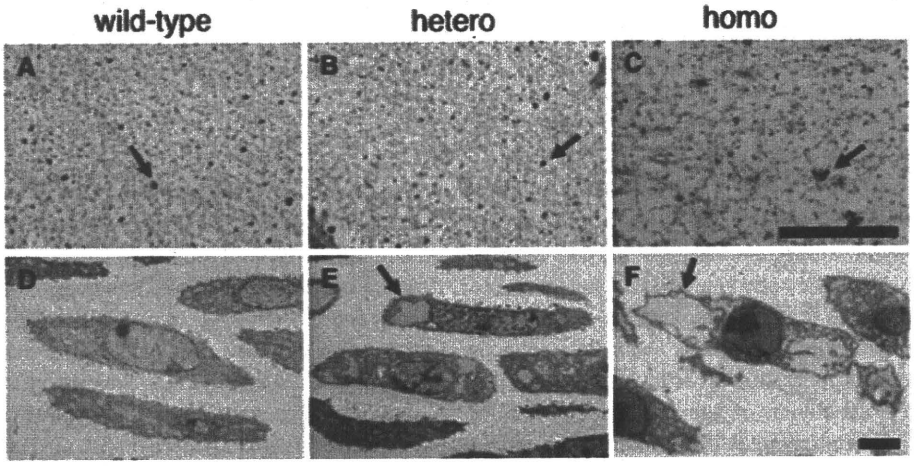

Fig. 5 Electron microscope images of the extracellular matrix (ECM) and chondrocytes from the proliferating zone in *Col2a1*^{Rgsc856} mutants at E18.5. **a–c** The images of the ECM are shown. *Arrows* indicate the proteoglycan aggregates. **d–f** The images of the chondrocytes are shown. *Arrows* show abnormally expanded rough endoplasmic reticulum (ER). Note that the collagen fibers of the homozygotes are markedly reduced (**c**). Abnormally expanded rough ER was found in the heterozygotes (**e**) and homozygotes (**f**). More expanded rough ER was evident in the homozygotes. *Scale bars* 1 μm (**a–c**) and 2 μm (**d–f**)

chondrocytes of *Col2a1*^{Rgsc856} mutants, secretion of mutant type II collagens into the extracellular space is disrupted, accompanied by abnormally expanded ER and upregulation of ER stress-related genes. These findings strongly suggested that ER stress is induced in the mutants.

Two mouse lines possessing an endogenous *Col2a1* mutation have been established. Until now, the *Dmm* mouse was the only known animal model with an endogenous C-propeptide mutation in *Col2a1* (Brown et al. 1981; Pace et al. 1997). Although the substituted amino acid in

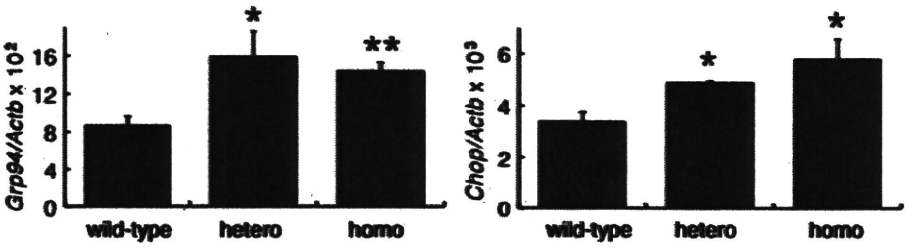

Fig. 6 Expression of mRNA encoding ER stress-related molecules in the rib cartilages of *Col2a1*^{Rgsc856} mutants at E18.5. GRP94 is an ER-resident chaperone and CHOP is a transcription factor used as an ER stress marker. Data were normalized with the expression levels of *Actb*. Data are expressed as the mean ± SE ($n = 5$). The p value was determined by one-way ANOVA followed by Bonferroni's test. * $p < 0.05$, ** $p < 0.01$. The same result was obtained from the independent experiment conducted using E19.5 embryos. The expression levels of the two genes in *Col2a1*^{Rgsc856} mutants were significantly higher than those in wild-type mice

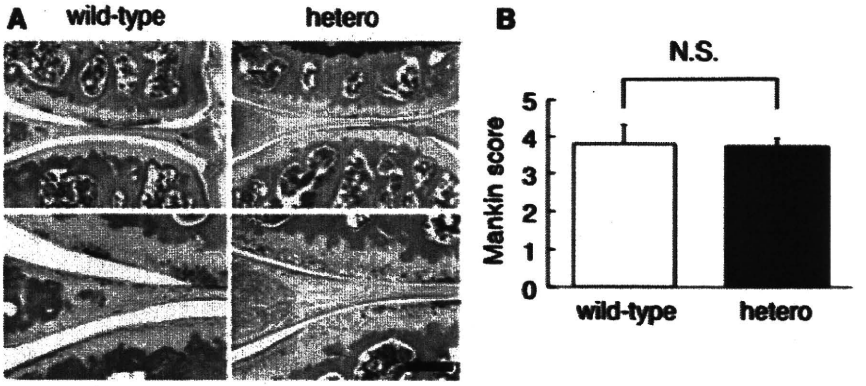

Fig. 7 Histological and histochemical evaluation (modified Mankin score) of articular cartilage in *Col2a1*^{Rgsc856} heterozygotes at 10 months of age. **a** Sections of the knee joint were stained with safranin O. **b** Modified Mankin score using the sections of knee joint. Data are expressed as the mean ± SE [wild type: $n = 5$ (two males and three females), *Col2a1*^{Rgsc856} heterozygous: $n = 4$ (two males and three females)]. The p value was determined by the Mann-Whitney U test. There was no significant difference between wild-type mice and *Col2a1*^{Rgsc856} heterozygotes. The same result was obtained in the analysis using sections from the elbow joint. *Scale bar* 100 μm

Col2a1^{Rgsc856} mutants (D1469) is located close to that in *Dmm* mice (K1448_T1449) in the C-propeptide region, there are phenotypic differences between the two mutants. At the newborn stage, the body size of *Dmm* heterozygotes is normal, but *Col2a1*^{Rgsc856} heterozygotes were significantly smaller than wild-type mice. *Dmm* heterozygotes show more severe degeneration of articular cartilage than wild-type mice at 10 months of age (Bomsta et al. 2006), but *Col2a1*^{Rgsc856} heterozygotes did not. Detailed phenotypic distinction between the two mutants is required. On the other hand, *Sedc* mice, a spontaneous mutant, carry a *Col2a1* missense mutation (c.3574C>T, p.R1192C) located near the C-terminus of the triple-helical domain (Donahue et al. 2003). Because this mutation causes the same amino acid substitution in SEDC patients, the mutant allele was named as *Sedc*. *Sedc* homozygotes are smaller than wild-type mice but can survive to adulthood and be fertile. Adult *Sedc* homozygotes exhibit mild skeletal dysplasia, retinoschisis, and hearing loss. *Sedc* mutants offer a valuable model to examine SEDC pathogenesis and the effect of mutations that substitute the amino acid residue in the X position of the Gly-X-Y repeat in the triple-helical domain. All human type II collagenopathies are inherited as an autosomal dominant trait; however, *Col2a1*^{Rgsc856}, *Dmm*, and *Sedc* heterozygotes exhibit very mild phenotypes, indicating that the effect of *COL2A1* mutations in humans is greater than that in mice. Several transgenic mouse lines that overexpress various mutant type II collagen molecules have also been studied (Arita et al. 2002; Maddox et al. 1997; Metsaranta et al. 1992). Because the large amount of mutant proteins from transgenes generally results in strong dominant-negative effects, most transgenic mouse lines exhibit embryonic lethality.

PLSD-T is a rare skeletal dysplasia characterized by platyspondyly, extremely short limbs, severe pelvic hypoplasia, and mild brachydactyly (Nishimura et al. 2004; Zankl et al. 2005). This disease is caused by heterozygous *COL2A1* mutations in the C-propeptide coding region and is generally lethal in the perinatal period, although a few long-term survivors have been reported. Because

of a number of phenotypic similarities, *Col2a1*^{Rgsc856} homozygotes offer a better model to examine PLSD-T pathogenesis. Indeed, the homozygotes showed skeletal features similar to those of PLSD-T patients. Furthermore, abnormally expanded rough ER was observed in both *Col2a1*^{Rgsc856} homozygotes and PLSD-T patients (Freisinger et al. 1996; Zankl et al. 2005). Our results from immunohistochemistry and electron microscope analyses indicated that in the homozygotes, mutant type II collagens accumulated in the expanded rough ER of chondrocytes and were poorly secreted into the extracellular space. The upregulation of ER stress-related genes (*Grp94* and *Chop*) suggested that ER stress was induced in *Col2a1*^{Rgsc856} mutants. These defects may disrupt the ECM network and zonal structure of growth plate cartilage and lead to severe skeletal dysplasia. The same molecular events may occur in PLSD-T pathogenesis.

The C-propeptide of fibrillar collagen plays a crucial role in triple-helical formation (Doege and Fessler 1986; Khoshnoodi et al. 2006). Once procollagen chains translocate into the lumen of the ER, they associate via their C-propeptides to form a trimer. This initial association is stabilized by intra- and interchain disulfide bonds. Triple-helix formation then occurs from the carboxyl- to the amino-terminal end. Intracellular accumulation of mutant proteins was observed in *Col2a1*^{Rgsc856} homozygotes, and an abnormally expanded ER was observed in both the homozygotes and the heterozygotes. These results indicated that the D1469 residue substituted in the *Col2a1*^{Rgsc856} allele is essential for the function of the C-propeptide. Intracellular accumulation of mutant proteins seems to be common to both *Col2a1*^{Rgsc856} and *Dmm* mutants (Fernandes et al. 2003; Seegmiller et al. 2008). Mutations in the *Col2a1*^{Rgsc856} and *Dmm* alleles are located close to each other, between the last two cysteine residues involved in the formation of intrachain disulfide bonds. The amino acid substitution in the *Dmm* allele (p.K1448_T1449delinsN) is predicted to change the local secondary structure from coil to strand (Fernandes et al. 2003). On the other hand, the substitution in the *Col2a1*^{Rgsc856} allele (p.D1469A) is predicted to cause a drastic polarity change. These varied effects may generate the phenotypic differences between the two mutants. C-propeptide is also known as chondrocalcin, which accumulates in the ECM of the hypertrophic zone of growth plate cartilage and seems to promote mineralization (Van der Rest et al. 1986); however, little else is known about this protein. *Col2a1*^{Rgsc856} mutants may also be useful to investigate C-propeptide functions as chondrocalcin.

Accumulation of misfolded mutant proteins in the ER induces ER stress (Ron and Walter 2007; Schroder and Kaufman 2005). In response to ER stress, eukaryotic cells increase transcription of genes encoding ER-resident chaperones such as BiP/GRP78 and GRP94; this system is termed the unfolded protein response (UPR). CHOP is a UPR-induced transcription factor used as an ER stress marker. The UPR is initially a response to relieve ER stress but if unresolved, it can lead to apoptotic cell death. Recently, misfolded mutant ECM proteins such as collagens, COMP, and matrilin 3 have been shown to induce ER stress and UPR (Bateman et al. 2009). It has been reported that the type I procollagen chains with the C-propeptide mutations identified in patients with osteogenesis imperfecta bind to BiP and upregulate the expression of both BiP and GRP94 (Chessler and Byers 1993). Type X procollagen chains with C-terminal noncollagenous (NC1) domain mutations identified in patients with metaphyseal chondrodysplasia (Schmid type) are unable to assemble into homotrimers and perform extracellular secretion (Wilson et al. 2005). These mutants have upregulated BiP and a spliced form of mRNA of the X-box binding protein 1 (*XBP1*), another key marker for the UPR. Activation of the UPR has been confirmed in transgenic mice expressing type X collagen with a 13-bp deletion within the NC1 domain (Tsang et al. 2007). Type II collagen chains with a triple-helical mutation—p.R989C—identified in SEDC patients upregulate and bind to BiP (Hintze et al. 2008). Furthermore, cells overexpressing the p.R989C mutant undergo apoptosis. It has also been reported that BiP and CHOP are upregulated in *Col2a1* transgenic mice expressing the triple-helical mutant p.G904C (Tsang et al. 2007). We demonstrated that *Grp94* and *Chop* expression was upregulated in *Col2a1*^{Rgsc856} mutants, suggesting that ER stress and the UPR is also induced in PLSD-T patients. It should be elucidated how the UPR and its downstream consequences, such as apoptosis and altered gene expression, relate to PLSD-T pathogenesis.

OA is the most common joint disease characterized by progressive degeneration of articular cartilage. *COL2A1* mutations have been identified in various types of skeletal dysplasias, some of which include OA in their phenotype (Loughlin 2001; Vikkula et al. 1993). Several studies suggest an association of *COL2A1* polymorphisms with OA (Ikeda et al. 2002). *Dmm* heterozygotes develop premature OA that is conspicuous from 3 through 22 months of age (Bomsta et al. 2006). In contrast, *Col2a1*^{Rgsc856} heterozygotes did not show a more severe degeneration of articular cartilage than wild-type mice at 10 months of age. Therefore, the *Dmm* allele should make a larger contribution to the OA phenotype than the *Col2a1*^{Rgsc856} allele. Combinational use of *Dmm* and *Col2a1*^{Rgsc856} heterozygotes may lead to an understanding of the relationship between the functional defect of the C-propeptide and the development of OA.

We have described skeletal and histological features of *Col2a1*^{Rgsc856} mutant mice that should become useful as a model of PLSD-T. Collection of more mutant alleles of

Col2a1 would lead to a better understanding of the mechanisms responsible for creating the great diversity of type II collagenopathies.

Acknowledgments We are grateful to Dr. S. Tominaga, Mrs. H. Yokoyama, and J. Nagano for their help with managing the animals, preparation of samples, identification of the mutation, and mouse genotyping. We also thank Charles River Laboratories Japan, Inc. for help with mouse breeding. This project was supported by grants-in-aid from the Ministry of Education, Culture, Sports and Science of Japan (contract grant Nos. 20390408 and 21249080), Research on Child Health and Development (contract grant No. 20-S-3), and Naito Foundation.

References

Ahmad NN, Ala-Kokko L, Knowlton RG, Jimenez SA, Weaver EJ, Maguire JI, Tasman W, Prockop DJ (1991) Stop codon in the procollagen II gene (*COL2A1*) in a family with the Stickler syndrome (arthro-ophthalmopathy). Proc Natl Acad Sci USA 88:6624–6627

Arita M, Li SW, Kopen G, Adachi E, Jimenez SA, Fertala A (2002) Skeletal abnormalities and ultrastructural changes of cartilage in transgenic mice expressing a collagen II gene (COL2A1) with a Cys for Arg-alpha1–519 substitution. Osteoarthr Cartil 10:808–815

Bateman JF, Boot-Handford RP, Lamande SR (2009) Genetic diseases of connective tissues: cellular and extracellular effects of ECM mutations. Nat Rev Genet 10:173–183

Bomsta BD, Bridgewater LC, Seegmiller RE (2006) Premature osteoarthritis in the Disproportionate micromelia (*Dmm*) mouse. Osteoarthr Cartil 14:477–485

Brown KS, Cranley RE, Greene R, Kleinman HK, Pennypacker JP (1981) Disproportionate micromelia (*Dmm*): an incomplete dominant mouse dwarfism with abnormal cartilage matrix. J Embryol Exp Morphol 62:165–182

Chessler SD, Byers PH (1993) BiP binds type I procollagen pro alpha chains with mutations in the carboxyl-terminal propeptide synthesized by cells from patients with osteogenesis imperfecta. J Biol Chem 268:18226–18233

Doege KJ, Fessler JH (1986) Folding of carboxyl domain and assembly of procollagen I. J Biol Chem 261:8924–8935

Donahue LR, Chang B, Mohan S, Miyakoshi N, Wergedal JE, Baylink DJ, Hawes NL, Rosen CJ, Ward-Bailey P, Zheng QY, Bronson RT, Johnson KR, Davisson MT (2003) A missense mutation in the mouse *Col2a1* gene causes spondyloepiphyseal dysplasia congenita, hearing loss, and retinoschisis. J Bone Miner Res 18:1612–1621

Fernandes RJ, Seegmiller RE, Nelson WR, Eyre DR (2003) Protein consequences of the *Col2a1* C-propeptide mutation in the chondrodysplastic *Dmm* mouse. Matrix Biol 22:449–453

Freisinger P, Bonaventure J, Stoess H, Pontz BF, Emmrich P, Nerlich A (1996) Type II collagenopathies: are there additional family members? Am J Med Genet 63:137–143

Hintze V, Steplewski A, Ito H, Jensen DA, Rodeck U, Fertala A (2008) Cells expressing partially unfolded R789C/p.R989C type II procollagen mutant associated with spondyloepiphyseal dysplasia undergo apoptosis. Hum Mutat 29:841–851

Hitotsumachi S, Carpenter DA, Russell WL (1985) Dose-repetition increases the mutagenic effectiveness of *N*-ethyl-*N*-nitrosourea in mouse spermatogonia. Proc Natl Acad Sci USA 82:6619–6621

Ikeda T, Mabuchi A, Fukuda A, Kawakami A, Ryo Y, Yamamoto S, Miyoshi K, Haga N, Hiraoka H, Takatori Y, Kawaguchi H, Nakamura K, Ikegawa S (2002) Association analysis of single nucleotide polymorphisms in cartilage-specific collagen genes with knee and hip osteoarthritis in the Japanese population. J Bone Miner Res 17:1290–1296

Inoue M, Sakuraba Y, Motegi H, Kubota N, Toki H, Matsui J, Toyoda Y, Miwa I, Terauchi Y, Kadowaki T, Shigeyama Y, Kasuga M, Adachi T, Fujimoto N, Matsumoto R, Tsuchihashi K, Kagami T, Inoue A, Kaneda H, Ishijima J, Masuya H, Suzuki T, Wakana S, Gondo Y, Minowa O, Shiroishi T, Noda T (2004) A series of maturity onset diabetes of the young, type 2 (MODY2) mouse models generated by a large-scale ENU mutagenesis program. Hum Mol Genet 13:1147–1157

Khoshnoodi J, Cartailler JP, Alvares K, Veis A, Hudson BG (2006) Molecular recognition in the assembly of collagens: terminal noncollagenous domains are key recognition modules in the formation of triple helical protomers. J Biol Chem 281: 38117–38121

Korkko J, Cohn DH, Ala-Kokko L, Krakow D, Prockop DJ (2000) Widely distributed mutations in the *COL2A1* gene produce achondrogenesis type II/hypochondrogenesis. Am J Med Genet 92:95–100

Kuivaniemi H, Tromp G, Prockop DJ (1997) Mutations in fibrillar collagens (types I, II, III, and XI), fibril-associated collagen (type IX), and network-forming collagen (type X) cause a spectrum of diseases of bone, cartilage, and blood vessels. Hum Mutat 9:300–315

Li SW, Prockop DJ, Helminen H, Fassler R, Lapvetelainen T, Kiraly K, Peltarri A, Arokoski J, Lui H, Arita M et al (1995) Transgenic mice with targeted inactivation of the *Col2a1* gene for collagen II develop a skeleton with membranous and periosteal bone but no endochondral bone. Genes Dev 9:2821–2830

Loughlin J (2001) Genetic epidemiology of primary osteoarthritis. Curr Opin Rheumatol 13:111–116

Maddox BK, Garofalo S, Smith C, Keene DR, Horton WA (1997) Skeletal development in transgenic mice expressing a mutation at Gly574Ser of type II collagen. Dev Dyn 208:170–177

Mankin HJ, Dorfman H, Lippiello L, Zarins A (1971) Biochemical and metabolic abnormalities in articular cartilage from osteoarthritic human hips. II. Correlation of morphology with biochemical and metabolic data. J Bone Joint Surg Am 53: 523–537

Masuya H, Inoue M, Wada Y, Shimizu A, Nagano J, Kawai A, Inoue A, Kagami T, Hirayama T, Yamaga A, Kaneda H, Kobayashi K, Minowa O, Miura I, Gondo Y, Noda T, Wakana S, Shiroishi T (2005a) Implementation of the modified-SHIRPA protocol for screening of dominant phenotypes in a large-scale ENU mutagenesis program. Mamm Genome 16:829–837

Masuya H, Shimizu K, Sezutsu H, Sakuraba Y, Nagano J, Shimizu A, Fujimoto N, Kawai A, Miura I, Kaneda H, Kobayashi K, Ishijima J, Maeda T, Gondo Y, Noda T, Wakana S, Shiroishi T (2005b) Enamelin (*Enam*) is essential for amelogenesis: ENU-induced mouse mutants as models for different clinical subtypes of human amelogenesis imperfecta (AI). Hum Mol Genet 14: 575–583

Masuya H, Nishida K, Furuichi T, Toki H, Nishimura G, Kawabata H, Yokoyama H, Yoshida A, Tominaga S, Nagano J, Shimizu A, Wakana S, Gondo Y, Noda T, Shiroishi T, Ikegawa S (2007) A novel dominant-negative mutation in *Gdf5* generated by ENU mutagenesis impairs joint formation and causes osteoarthritis in mice. Hum Mol Genet 16:2366–2375

Metsaranta M, Garofalo S, Decker G, Rintala M, de Crombrugghe B, Vuorio E (1992) Chondrodysplasia in transgenic mice harboring a 15-amino-acid deletion in the triple helical domain of pro alpha 1(II) collagen chain. J Cell Biol 118:203–212

Mortier GR, Weis M, Nuytinck L, King LM, Wilkin DJ, De Paepe A, Lachman RS, Rimoin DL, Eyre DR, Cohn DH (2000) Report of five novel and one recurrent *COL2A1* mutation with analysis of genotype-phenotype correlation in patients with a lethal type II collagen disorder. J Med Genet 37:263–271

Myllyharju J, Kivirikko KI (2004) Collagens, modifying enzymes and their mutations in humans, flies and worms. Trends Genet 20:33–43

Nishimura G, Nakashima E, Mabuchi A, Shimamoto K, Shimamoto T, Shimao Y, Nagai T, Yamaguchi T, Kosaki R, Ohashi H, Makita Y, Ikegawa S (2004) Identification of *COL2A1* mutations in platyspondylic skeletal dysplasia, Torrance type. J Med Genet 41:75–79

Nishimura G, Haga N, Kitoh H, Tanaka Y, Sonoda T, Kitamura M, Shirahama S, Itoh T, Nakashima E, Ohashi H, Ikegawa S (2005) The phenotypic spectrum of *COL2A1* mutations. Hum Mutat 26:36–43

Nolan PM, Kapfhamer D, Bucan M (1997) Random mutagenesis screen for dominant behavioral mutations in mice. Methods 13:379–395

Olsen BR (1995) New insights into the function of collagens from genetic analysis. Curr Opin Cell Biol 7:720–727

Pace JM, Li Y, Seegmiller RE, Teuscher C, Taylor BA, Olsen BR (1997) Disproportionate micromelia (Dmm) in mice caused by a mutation in the C-propeptide coding region of *Col2a1*. Dev Dyn 208:25–33

Ron D, Walter P (2007) Signal integration in the endoplasmic reticulum unfolded protein response. Nat Rev Mol Cell Biol 8:519–529

Saito A, Hino S, Murakami T, Kanemoto S, Kondo S, Saitoh M, Nishimura R, Yoneda T, Furuichi T, Ikegawa S, Ikawa M, Okabe M, Imaizumi K (2009) Regulation of endoplasmic reticulum stress response by a BBF2H7-mediated Sec23a pathway is essential for chondrogenesis. Nat Cell Biol 11: 1197–1204

Schroder M, Kaufman RJ (2005) ER stress and the unfolded protein response. Mutat Res 569:29–63

Seegmiller RE, Bomsta BD, Bridgewater LC, Niederhauser CM, CMontaño C, Sudweeks S, Eyre DR, Fernandes RJ (2008) The heterozygous disproportionate micromelia (*Dmm*) mouse: morphological changes in fetal cartilage precede postnatal dwarfism and compared with lethal homozygotes can explain the mild phenotype. J Histochem Cytochem 56:1003–1011

Tsang KY, Chan D, Cheslett D, Chan WC, So CL, Melhado IG, Chan TW, Kwan KM, Hunziker EB, Yamada Y, Bateman JF, Cheung KM, Cheah KS (2007) Surviving endoplasmic reticulum stress is coupled to altered chondrocyte differentiation and function. PLoS Biol 5:e44

Unger S, Korkko J, Krakow D, Lachman RS, Rimoin DL, Cohn DH (2001) Double heterozygosity for pseudoachondroplasia and spondyloepiphyseal dysplasia congenita. Am J Med Genet 104: 140–146

Van der Rest M, Rosenberg LC, Olsen BR, Poole AR (1986) Chondrocalcin is identical with the C-propeptide of type II procollagen. Biochem J 237:923–925

van der Sluijs JA, Geesink RG, van der Linden AJ, Bulstra SK, Kuyer R, Drukker J (1992) The reliability of the Mankin score for osteoarthritis. J Orthop Res 10:58–61

Vikkula M, Palotie A, Ritvaniemi P, Ott J, Ala-Kokko L, Sievers U, Aho K, Peltonen L (1993) Early-onset osteoarthritis linked to the type II procollagen gene. Detailed clinical phenotype and further analyses of the gene. Arthritis Rheum 36:401–409

Wilson R, Freddi S, Chan D, Cheah KS, Bateman JF (2005) Misfolding of collagen X chains harboring Schmid metaphyseal chondrodysplasia mutations results in aberrant disulfide bond formation, intracellular retention, and activation of the unfolded protein response. J Biol Chem 280:15544–15552

Winterpacht A, Hilbert M, Schwarze U, Mundlos S, Spranger J, Zabel BU (1993) Kniest and Stickler dysplasia phenotypes caused by collagen type II gene (*COL2A1*) defect. Nat Genet 3:323–326

Zabel B, Hilbert K, Stoss H, Superti-Furga A, Spranger J, Winterpacht A (1996) A specific collagen type II gene (*COL2A1*) mutation presenting as spondyloperipheral dysplasia. Am J Med Genet 63:123–128

Zankl A, Neumann L, Ignatius J, Nikkels P, Schrander-Stumpel C, Mortier G, Omran H, Wright M, Hilbert K, Bonafe L, Spranger J, Zabel B, Superti-Furga A (2005) Dominant negative mutations in the C-propeptide of *COL2A1* cause platyspondylic lethal skeletal dysplasia, torrance type, and define a novel subfamily within the type 2 collagenopathies. Am J Med Genet A 133A:61–66

THE JOURNAL OF BIOLOGICAL CHEMISTRY VOL. 285, NO. 45, pp. 34885–34898, November 5, 2010

Seeded Aggregation and Toxicity of α-Synuclein and Tau

CELLULAR MODELS OF NEURODEGENERATIVE DISEASES[*][S]

Received for publication, May 26, 2010, and in revised form, August 17, 2010 Published, JBC Papers in Press, August 30, 2010, DOI 10.1074/jbc.M110.148460

Takashi Nonaka[‡1], **Sayuri T. Watanabe**[‡§], **Takeshi Iwatsubo**[§¶], **and Masato Hasegawa**[‡2]

From the [‡]*Department of Molecular Neurobiology, Tokyo Institute of Psychiatry, Tokyo 156-8585 and the* [§]*Department of Neuropathology and Neuroscience, Graduate School of Pharmaceutical Science, and* [¶]*Department of Neuropathology, Graduate School of Medicine, University of Tokyo, Tokyo 113-0033, Japan*

The deposition of amyloid-like filaments in the brain is the central event in the pathogenesis of neurodegenerative diseases. Here we report cellular models of intracytoplasmic inclusions of α-synuclein, generated by introducing nucleation seeds into SH-SY5Y cells with a transfection reagent. Upon introduction of preformed seeds into cells overexpressing α-synuclein, abundant, highly filamentous α-synuclein-positive inclusions, which are extensively phosphorylated and ubiquitinated and partially thioflavin-positive, were formed within the cells. SH-SY5Y cells that formed such inclusions underwent cell death, which was blocked by small molecular compounds that inhibit β-sheet formation. Similar seed-dependent aggregation was observed in cells expressing four-repeat Tau by introducing four-repeat Tau fibrils but not three-repeat Tau fibrils or α-synuclein fibrils. No aggregate formation was observed in cells overexpressing three-repeat Tau upon treatment with four-repeat Tau fibrils. Our cellular models thus provide evidence of nucleation-dependent and protein-specific polymerization of intracellular amyloid-like proteins in cultured cells.

The conversion of certain soluble peptides and proteins into insoluble filaments or misfolded amyloid proteins is believed to be the central event in the etiology of a majority of neurodegenerative diseases (1–4). Alzheimer disease (AD)[3] is characterized by the deposition of two kinds of filamentous aggregates, extracellular deposits of β-amyloid plaques composed of amyloid β (Aβ) peptides, and intracellular neurofibrillary lesions consisting of hyperphosphorylated Tau. In Parkinson disease (PD) and dementia with Lewy bodies (DLB), filamentous inclusions consisting of hyperphosphorylated α-synuclein (α-syn) are accumulated in degenerating neurons (5). The deposition of prion proteins in synapses and extracellular spaces is the defining characteristic of Creutzfeldt-Jakob disease and other prion diseases (3). The identification of genetic defects associated with early onset AD, familial PD, frontotemporal dementia, parkinsonism linked to chromosome 17 (caused by Tau mutation and deposition), and familial Creutzfeldt-Jakob disease has led to the hypothesis that the production and aggregation of these proteins are central to the development of neurodegeneration. Fibrils formed of Aβ display a prototypical cross-β-structure characteristic of amyloid (6), as do many other types of filaments deposited in the extracellular space in systemic or organ-specific amyloidoses (7), including prion protein deposits (8). Filaments assembled from α-syn (9) and from Tau filaments (10) were also shown to possess cross-β-structure, as were synthetic filaments derived from exon 1 of huntingtin with 51 glutamines (11). It therefore seems appropriate to consider neurodegenerative disorders developing intracellular deposits of amyloid-like proteins as brain amyloidosis. The accumulation and propagation of extracellular amyloid proteins are believed to occur through nucleation-dependent polymerization (12, 13). However, it has been difficult to establish the relevance of this process in the *in vivo* situation because of the lack of a suitable cell culture model or method to effectively introduce seeds into cells. For example, it has not yet been possible to generate *bona fide* fibrous inclusions reminiscent of Lewy bodies as a model of PD by overexpressing α-syn in neurons of transgenic animals. Here, we describe a novel method for introducing amyloid seeds into cultured cells using lipofection, and we present experimental evidence of seed-dependent polymerization of α-syn, leading to the formation of filamentous protein deposits and cell death. This was also clearly demonstrated in cells expressing different Tau isoforms by introducing the corresponding Tau fibril seeds.

EXPERIMENTAL PROCEDURES

Chemicals and Antibodies—A phosphorylation-independent antibody Syn102 and monoclonal and polyclonal antibodies against a synthetic phosphopeptide of α-syn ($Ser(P)^{129}$) were used as described previously (5). Polyclonal anti-ubiquitin antibody was obtained from Dako. Polyclonal anti-Tau $Ser(P)^{396}$ was obtained from Calbiochem. Monoclonal anti-α-tubulin and anti-HA clone HA-7 were obtained from Sigma. Lipofectamine was purchased from Invitrogen. Monoclonal

* This work was supported by grants-in-aid for scientific research on Priority Areas, Research on Pathomechanisms of Brain Disorders (to T. I. and M. H.) and Grant-in-aid for Scientific Research (C) 19590297 and 22500345 (to T. N.) from the Ministry of Education, Culture, Sports, Science, and Technology of Japan.

[S] The on-line version of this article (available at http://www.jbc.org) contains supplemental Figs. S1–S5.

[1] To whom correspondence may be addressed: Dept. of Molecular Neurobiology, Tokyo Institute of Psychiatry 2-1-8 Kamikitazawa, Setagaya-ku, Tokyo 156-8585, Japan. Tel.: 81-3-3304-5701; Fax: 81-3-3329-8035; E-mail: nonaka-tk@igakuken.or.jp.

[2] To whom correspondence may be addressed: Dept. of Molecular Neurobiology, Tokyo Institute of Psychiatry 2-1-8 Kamikitazawa, Setagaya-ku, Tokyo 156-8585, Japan. Tel.: 81-3-3304-5701; Fax: 81-3-3329-8035; E-mail: hasegawa-ms@igakuken.or.jp.

[3] The abbreviations used are: AD, Alzheimer disease; Aβ, amyloid β; PD, Parkinson disease; DLB, dementia with Lewy bodies; α-syn, α-synuclein; 3R1N, three-repeat Tau isoform with one amino-terminal insert; 4R1N, four-repeat Tau isoform with one amino-terminal insert; LA, Lipofectamine; LDH, lactate dehydrogenase.

anti-Tau T46 was from Zymed Laboratories Inc.. AT100 and HT7 antibodies were obtained from Innogenetics.

Preparation of α-Syn Seed, Oligomers, and Tau Fibrils—Human α-syn cDNA in bacterial expression plasmid pRK172 was used to produce recombinant protein (14). Wild-type (WT) or carboxyl-terminally HA-tagged α-syn was expressed in *Escherichia coli* BL21 (DE3) and purified as described (15). To obtain α-syn fibrils, α-syn (5–10 mg/ml) was incubated at 37 °C for 4 days with continuous shaking. The samples were diluted with 5 volumes of 30 mM Tris-HCl buffer (pH 7.5) and ultracentrifuged at 110,000 × *g* for 20 min at 25 °C. The pellets were resuspended in 30 mM Tris-HCl buffer (pH 7.5) and sonicated twice for 5 s each. The protein concentration was determined as described, and this preparation was used as Seed αS. In the case of α-syn oligomers, α-syn (10 mg/ml) was incubated at 37 °C for 3 days in the presence of 10 mM exifone. After incubation, the mixture was ultracentrifuged at 110,000 × *g* for 20 min at 25 °C. The supernatant was desalted by Sephadex G-25 (Amersham Biosciences) column chromatography, and eluted fractions (α-syn oligomers) were analyzed by reversed-phase HPLC, SDS-PAGE, and immunoblot analysis. Recombinant human three-repeat Tau isoform with one amino-terminal insert (3R1N) and four-repeat Tau isoform with one amino-terminal insert (4R1N) monomer and corresponding fibrils were prepared as described previously (16, 17).

Introduction of Proteins into Cells—Human neuroblastoma SH-SY5Y cells obtained from ATCC were cultured in DMEM/F-12 medium with 10% FCS. Cells at ~30–50% confluence in 6-well plates were treated with 200 μl of Opti-MEM containing 2 μg of the seed α-syn WT (Seed αS); HA-tagged α-syn (Seed-HA); α-syn monomers, oligomers; or Tau 3R1N or 4R1N fibrils; and 5 μl of Lipofectamine (LA) for 3 h at 37 °C. The medium was changed to DMEM/F-12, and culture was continued for 14 h. The cells were collected by treatment with 0.5 ml of 0.25% trypsin for 10 min at 37 °C, followed by centrifugation (1,800 × *g*, 5 min) and washing with PBS. The cellular proteins were extracted with 100 μl of homogenization buffer containing 50 mM Tris-HCl, pH 7.5, 0.15 M NaCl, 5 mM EDTA, and a mixture of protease inhibitors by sonication. After ultracentrifugation at 290,000 × *g* for 20 min at 4 °C, the supernatant was collected as a Tris-soluble fraction, and the protein concentration was determined by BCA assay. The pellet was solubilized in 100 μl of SDS-sample buffer. Both Tris-soluble and insoluble fractions were analyzed by immunoblotting with appropriate antibodies as indicated (15, 18).

Cell Culture Model of Seed-dependent Polymerization of α-Syn or Tau—α-Syn or Tau 3R1N or 4R1N was transiently overexpressed in SH-SY5Y cells by transfection of 1 μg of wild-type human α-syn cDNA in pcDNA3 (pcDNA3-α-syn) or human Tau cDNA in pcDNA3 (pcDNA3-Tau 3R1N or 4R1N) with 3 μl of FuGENE6 (Roche Applied Science) in 100 μl of Opti-MEM, followed by culture for 14 h. Under our experimental conditions, the efficiency of transfection with pEGFP-C1 vector was 20–30%. The cells were washed with PBS once, and then Seed αS, Seed-HA, Seed 3R1N, or Seed 4R1N was introduced with Lipofectamine as described above. The medium was changed to DMEM/F-12, and culture was continued for ~2–3 days. Cells were harvested in the presence of trypsin to digest extracellular cell-associated α-syn fibrils. The cellular proteins were differentially extracted and immunoblotted with the indicated antibodies, as described (18).

Confocal Microscopy—SH-SY5Y cells on coverslips were transfected with pcDNA3-α-syn and cultured for 14 h as described above, and then Seed αS was introduced, and culture was continued for ~1–2 days. After fixation with 4% paraformaldehyde, the cells were stained with appropriate primary and secondary antibodies as described previously (18). For thioflavin S staining, the cells were incubated with 0.05% thioflavin S at room temperature for 5 min. Fluorescence was analyzed with a laser-scanning confocal fluorescence microscope (LSM5Pascal, Carl Zeiss).

Immunoelectron Microscopy—For electron microscopy, cells overexpressing α-syn were transfected with Seed αS, cultured for 2 days, fixed in 0.1 M phosphate buffer containing 4% glutaraldehyde for 12 h, and then processed and embedded in LR White resin (London Resin, Reading, UK). Ultrathin sections were stained with uranyl acetate for investigation. Immunolabeling of the inclusions was performed by means of an immunogold-based postembedding procedure. Sections were blocked with 10% calf serum, incubated overnight on grids with anti-Ser(P)[129] antibody at a dilution of 1:100, rinsed, then reacted with secondary antibody conjugated to 10-nm gold particles (E-Y Laboratories, San Mateo, CA) (1:10), rinsed again and stained with uranyl acetate.

Immunoelectron microscopic analysis of α-syn or Tau filaments extracted from cells was performed as follows. Cells overexpressing α-syn or Tau were transfected with Seed αS or Seed Tau, respectively. After incubation for 3 days, they were harvested, suspended in 200 μl of 10 mM Tris-HCl, pH 7.4, 1 mM EGTA, 10% sucrose, 0.8 M NaCl) and sonicated. The lysates were centrifuged at 20,400 × *g* for 20 min at 4 °C. The supernatant was recovered, and Sarkosyl was added (final 1%, v/v). The mixtures were incubated at room temperature for 30 min and then centrifuged at 113,000 × *g* for 20 min. The resulting pellets were suspended in 30 mM Tris-HCl, pH 7.5, placed on collodion-coated 300-mesh copper grids, and stained with the indicated antibodies and 2% (v/v) phosphotungstate. Micrographs were recorded on a JEOL 1200EX electron microscope.

Cell Death Assay—Cell death assay was performed using a CytoTox 96 non-radioactive cytotoxicity assay kit (Promega). TUNEL staining was performed using an *in situ* cell death detection kit (Roche Applied Science).

Assay of Proteasome Activity—SH-SY5Y cells transfected with pcDNA3-α-syn and Seed αS were cultured for 3 days or treated with 20 μM MG132 for 4 h. Cells were harvested, and cytosolic fraction was prepared as follows. Cells were resuspended in 100 μl of phosphate-buffered saline (PBS) and disrupted by sonication, and then insoluble material was removed by ultracentrifugation at 290,000 × *g* for 20 min at 4 °C. The supernatant was assayed for proteasome activity by using a fluorescent peptide substrate, benzyloxycarbonyl-Leu-Leu-Glu-7-amido-4-methylcoumarin (Peptide Institute, Inc.). 7-Amino-4-methylcoumarin release was measured fluorometrically (excitation at 365 nm; emission at 460 nm). In a green fluorescent protein (GFP) reporter assay of proteasome activity in living cells by confocal laser microscopy, SH-SY5Y cells trans-

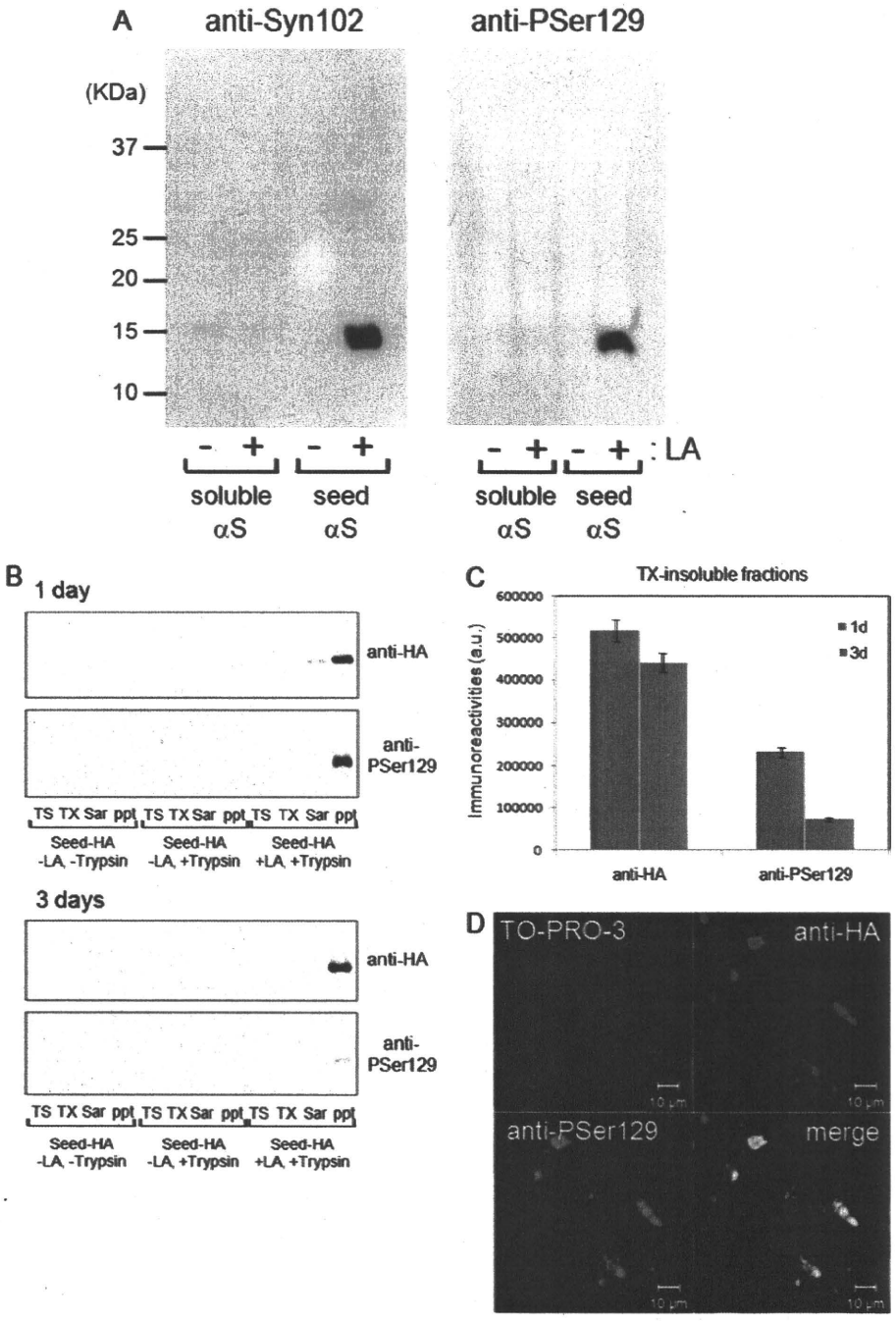

FIGURE 1. **Introduction of seed α-syn into cultured cells with Lipofectamine reagent.** *A*, purified recombinant α-syn (soluble form; 2 μg) and filaments (2 μg) were sonicated and then incubated with LA. The protein-LA complexes were dispersed in Opti-MEM and added to SH-SY5Y cells. After 14 h of culture, the cells were collected and sonicated in SDS sample buffer. After boiling, the samples were analyzed by immunoblotting with a phosphorylation-dependent anti-α-syn Ser(P)^{129} (*PSer129*) (*right*) or a phosphorylation-independent antibody, Syn102 (*left*). *B* and *C*, carboxyl-terminally HA-tagged α-syn fibril seeds (*Seed-HA*) were transduced into cells by the use of LA. After incubation for 1 day (*1d*) or 3 days (*3d*), cells were harvested with or without trypsin, and proteins were differentially extracted from the cells with Tris-HCl (*TS*), Triton X-100 (*TX*), and Sarkosyl (*Sar*), leaving the pellet (*ppt*). Immunoblot analyses of lysates using anti-HA and anti-Ser(P)^{129} are shown. The immunoreactive band positive for anti-HA or anti-Ser(P)^{129} in the Triton X-100-insoluble fraction was quantified. The results are expressed as means ± S.E. ($n = 3$). *D*, confocal laser microscopic analysis of cells treated with Seed-HA in the presence of LA. Cells were transduced with 2 μg of Seed-HA using 5 μl of LA. After a 48-h incubation, cells were fixed and immunostained with anti-Ser(P)^{129} (*green*) and anti-HA (*red*) and counterstained with TO-PRO-3 (*blue*).

fected with pcDNA3-α-syn (1 μg) and GFP-CL1 (0.3 μg) using FuGENE6 and then transfected with Seed αS were grown on coverslips for 2 days or treated with 20 μM MG132 for 6 h (19). These cells were analyzed using a laser-scanning confocal fluorescence microscope (LSM5Pascal, Carl Zeiss).

Statistical Analysis—The *p* values for the description of the statistical significance of differences were calculated by means of the unpaired, two-tailed Student's *t* test using GraphPad Prism 4 software (GraphPad Software).

RESULTS

Introduction of Seed α-Syn into Cultured Cells Using Lipofectamine Reagent—Cellular overexpression of α-syn by itself does not lead to fibrillization of α-syn in a form that resembles Lewy bodies. This prompted us to examine whether or not introduction of preformed aggregation seeds of α-syn (Seed αS) would elicit fibril formation. To introduce Seed αS into SH-SY5Y cells in a non-invasive manner, we tried several reagents used for transporting proteins or plasmid DNA into cells and found that LA, a cationic gene introducer, enables the introduction of Seed αS into SH-SY5Y cells. We were not able to detect any introduced α-syn monomer or fibrils following the simple addition of protein preparations to the culture medium, notwithstanding a previous report on this approach (20). The insoluble α-syn formed following LA-mediated Seed αS introduction was detected as buffer-insoluble α-syn in cell lysates (Fig. 1*A*). The insoluble α-syn was phosphorylated at Ser^{129} upon introduction into cells (Fig. 1*A*), indicating that Seed αS was incorporated in cells and phosphorylated intracellularly. Cells were harvested in the presence of trypsin to digest extracellular cell-associated α-syn fibrils. The optimal ratio of LA to Seed αS was about 5 μl to 2 μg of protein in 6-well plates. This treatment effectively introduced Seed αS not only into SH-SY5Y cells but also into several other types of cells examined, including Chinese hamster ovary cells and human embryonic kidney 293T cells (data not shown). In sharp contrast, soluble α-syn (either monomeric or oligomeric forms) was not introduced into the

cells by the same treatment (Figs. 1*A* and 4), suggesting that the LA treatment works exclusively for the internalization of insoluble α-syn aggregates.

These results strongly suggest that α-syn fibrils are incorporated with the aid of LA but do not exclude the possibility that extracellular α-syn fibrils may induce aggregation of endogenous α-syn without incorporation. To confirm that the extracellular α-syn fibril seeds are internalized into cells by LA, we performed the transduction of preformed carboxyl-terminally HA-tagged α-syn fibril seeds (Seed-HA) instead of non-tagged

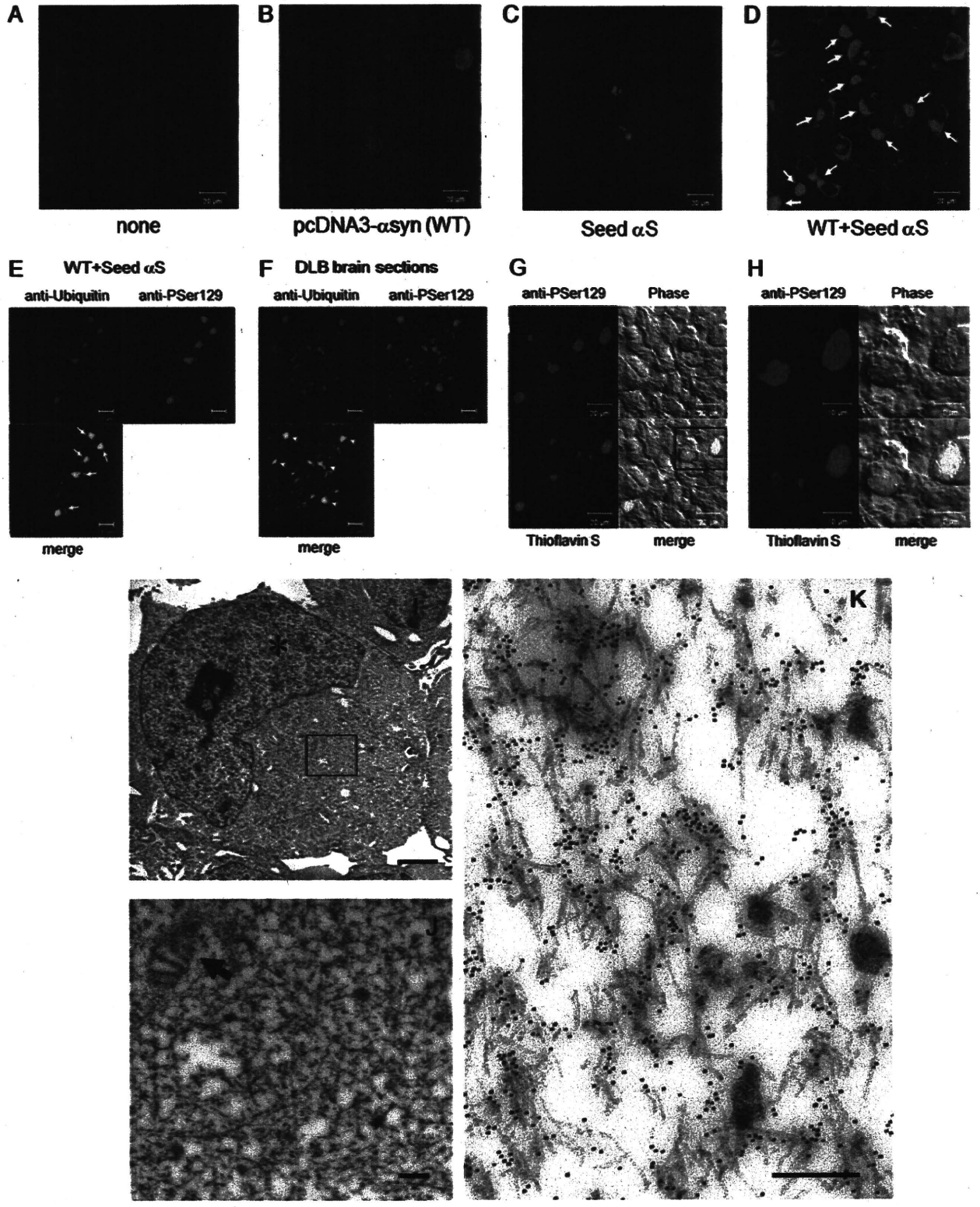

α-syn seeds. As shown in Fig. 1, *B* and *C*, time course experiments revealed that Seed-HA was also incorporated into cells in the presence of LA and could be detected with both anti-HA antibody and a phospho-α-syn-specific antibody (anti-Ser(P)^{129}), even 3 days after infection. Confocal microscopic analyses also indicated that Seed-HA was phosphorylated at Ser^{129} intracellularly. All anti-Ser(P)^{129}-positive dotlike structures were also stained with anti-HA, indicating that no endogenously phosphorylated α-syn aggregates are present in the cells (Fig. 1*D* and supplemental Fig. S1*C*).

Establishment of a Cell Culture Model for Nucleation-dependent Polymerization of α-Syn—Although introduction of the seed α-syn into cells was accompanied with phosphorylation, no further dramatic change was observed. Because the level of endogenous α-syn was relatively low in SH-SY5Y cells, we introduced non-tagged or HA-tagged seeds into cells transiently overexpressing α-syn. After 3 days of culture, immunocytochemistry for α-syn revealed a diffuse (Fig. 2*B*) or dotlike (Fig. 2*C*) pattern of cytoplasmic labeling by anti-Ser(P)^{129} in cells transfected with wild-type α-syn without seeds or in non-overexpressing cells with Seed αS, respectively. Surprisingly, however, in cells transfected with both pcDNA3-α-syn and Seed αS, we observed abundant round inclusions that occupied the cytoplasm and displaced the nucleus, with morphology highly reminiscent of cortical-type Lewy bodies observed in human brain (Fig. 2*D*). The size of the α-syn-positive inclusions was ~10 μm in diameter (Fig. 2*D*), which is similar to that of the Lewy bodies detected in the brains of patients with dementia with Lewy bodies. Similarly, when cells expressing α-syn were transfected with Seed-HA, abundant phosphorylated α-syn-positive cells were also detected (supplemental Fig. S1*D*).

We next examined the status of ubiquitin, which is positive in most types of intracellular filamentous inclusions, including Lewy bodies, in neurodegenerative disease brains. As shown in Fig. 2*E*, we found that almost all intracellular inclusions labeled with anti-Ser(P)^{129} were also positive for ubiquitin, as is the case for Lewy bodies in the cortex of human DLB brain (Fig. 2*F*). Furthermore, the juxtanuclear Ser(P)^{129}-positive, Lewy body-like inclusions were also positively labeled with thioflavin S, a fluorescent dye that specifically intercalates within structures rich in β-pleated sheet conformation (Fig. 2, *G* and *H*), indicating that the inclusions contain β-sheet-rich filamentous aggregates. Electron microscopic analysis of cells transfected with both wild-type α-syn and the seeds revealed that the inclusions are composed of filamentous structures ~10 nm in diameter that are often covered with granular materials (Fig. 2, *I* and *J*). The filamentous structures were randomly oriented within the cytoplasm of these cells, forming a meshwork-like profile, and were frequently intermingled with mitochondria (Fig. 2, *I* and *J*), being highly reminiscent of human cortical Lewy bodies. Immunoelectron microscopy showed that the filaments were densely decorated with anti-Ser(P)^{129} (Fig. 2*K*), demonstrating that they were composed of phosphorylated α-syn.

To biochemically validate this cellular model and to investigate further the molecular mechanisms underlying nucleation-dependent aggregation within cells, we differentially extracted α-syn from these cells using detergents of various strengths and analyzed the extracts by immunoblotting with anti-Syn102 and -Ser(P)^{129} antibodies. The levels of α-syn in the Sarkosyl-soluble and -insoluble fractions (total α-syn and α-syn phosphorylated at Ser^{129}, respectively) were dramatically increased in cells transfected with both wild-type α-syn and the seeds (*WT + Seed αS* in Fig. 3, *A* and *B*). To distinguish endogenous α-syn from exogenous α-syn fibrils, we used LA to transduce Seed-HA into cells overexpressing α-syn. Immunoblot analyses of these cells showed that HA-tagged α-syn with slower mobility than non-tagged α-syn was detected in the Sarkosyl-insoluble pellets as phosphorylated forms by anti-HA and anti-Ser(P)^{129} antibodies in cells treated with Seed-HA + LA (Fig. 3, *C–E*). Interestingly, in cells expressing α-syn (WT) treated with Seed-HA + LA, much more abundant non-tagged α-syn was detected in the Triton X-100- and Sarkosyl-insoluble fractions as phosphorylated forms with a smaller amount of the HA-α-syn. We also performed a dose dependence experiment with Seed-HA in cells expressing α-syn. As shown in supplemental Fig. S2, immunoreactive levels of Triton X-100-insoluble phosphorylated α-syn increased in parallel with an increase in the amount of Seed-HA. Furthermore, we tested whether Tau protein forms intracellular aggregates in the presence of α-syn seeds instead of Tau seeds. We found that Tau was not aggregated with Seed-HA, confirming that intracellular aggregate formation of soluble α-syn is specific to and dependent on fibril seeds of the same protein (supplemental Fig. S3). This nucleation-dependent polymerization of α-syn in cells was greater at 3 days than at 1 day after transduction of the seeds (Fig. 3*F*).

Negative stain electron microscopic observation of Sarkosyl-insoluble fractions of the cells harboring inclusions revealed anti-Syn102 and Ser(P)^{129}-positive filaments of ~5–10-nm width (Fig. 3, *G* and *H*) that are highly reminiscent of those derived from human α-synucleinopathy brains (21). Such filaments were never detected in the Sarkosyl-insoluble fraction of cells solely overexpressing α-syn (data not shown). These results indicated that the biochemical characteristics of α-syn accumulated in cells forming the Lewy body-like inclusions

FIGURE 2. **Confocal laser and electron microscopic analyses of α-syn inclusions in plasmid-derived α-syn-expressing cells treated with seed α-syn.** *A–D*, confocal laser microscopic analyses of control SH-SY5Y cells transfected with pcDNA3 vector and Lipofectamine alone (*A*), cells transfected with pcDNA3-α-syn (*WT*) (*B*), cells transduced with the seed α-syn (*Seed αS*) (*C*), and cells transfected with both pcDNA3-α-syn and Seed αS (*WT + Seed αS*) (*D*), immunostained with anti-Ser(P)^{129} (*green*), and counterstained with TO-PRO-3 (*blue*). The *arrows* indicate cytoplasmic round inclusions stained with anti-Ser(P)^{129} (*PSer129*). *Scale bars*, 20 μm. *E–F*, comparison of confocal images of cells transfected with both α-syn plasmid and Seed αS (*E*) and tissue sections from DLB brains (*F*) using anti-Ser(P)^{129} (*green*) and anti-ubiquitin antibodies (*red*). Cytoplasmic inclusions in transfected cells (*arrows*) are positive for ubiquitin, like Lewy bodies (*arrowheads*) in DLB brains. *Scale bars*, 20 μm. *G* and *H*, confocal microscopic images of cells transfected with both pcDNA3-α-syn and Seed αS. Cells were stained with 0.05% Thioflavin S (*green*) and anti-Ser(P)^{129} antibody (*red*). The *boxed area* on the *left* is shown in the *right panel*. *Scale bars*, 20 μm on the *left* and 10 μm on the *right*. *I* and *J*, electron microscopic analyses of cells transfected with both pcDNA3-α-syn and Seed αS. High magnification of the boxed area in *I* is shown in *J*. An *asterisk* or *arrow* indicates a nucleus or mitochondrion, respectively. *Scale bars*, 2 μm in *I* and 200 nm in *J*. *K*, immunoelectron microscopic observation of cells transfected with both pcDNA3-α-syn and Seed αS using a polyclonal antibody against phosphorylated Ser^{129} of α-syn. *Scale bar*, 200 nm.

were very similar to those of α-syn deposited in the brains of patients with α-synucleinopathies, including PD and DLB.

Because the idea has been gaining ground that transient oligomers, rather than mature fibrils, are responsible for cytotoxicity, we examined whether soluble oligomers could be introduced into cells in the same manner as fibril seeds by means of LA treatment and whether they could function as seeds for intracellular α-syn aggregate formation. As shown in Fig. 4, *A* and *B*, we purified stable α-syn oligomers from recombinant α-syn treated with exifone, an inhibitor of *in vitro* α-syn aggregation, which is thought to inhibit filament formation of α-syn by stabilizing SDS-resistant soluble oligomers (22, 23). Then cells expressing α-syn or mock plasmid were treated with a mixture of the oligomer fraction (5 μg) and LA and incubated for 3 days. Immunoblot analyses of lysates of these cells did not detect any SDS-resistant soluble oligomeric α-syn, and the levels of phosphorylated α-syn in the Sarkosyl-soluble and -insoluble fractions showed no increase (Fig. 4, *C* and *D*). On the other hand, we observed phosphorylated and deposited α-syn in the Sarkosyl-soluble and -insoluble fractions in cells expressing α-syn treated with Seed αS (Fig. 4, *C* and *D*). These results showed that SDS-resistant soluble oligomer of α-syn could not be introduced into cultured cells in the same manner as monomeric α-syn and/or could not function as seeds for intracellular α-syn aggregation.

Mutagenic Analysis of Nucleation-dependent Assembly of α-Syn—To investigate further the nucleation-dependent polymerization of α-syn, we analyzed the polymerization of α-syn mutated or truncated at various residues or subdomains that are believed to be crucial for its aggregation. Overexpression of A53T familial Parkinson mutant α-syn, which is readily fibrillogenic *in vitro*, in the presence of Seed αS moderately increased the accumulation and phosphorylation of α-syn in the Sarkosyl-soluble and insolu-

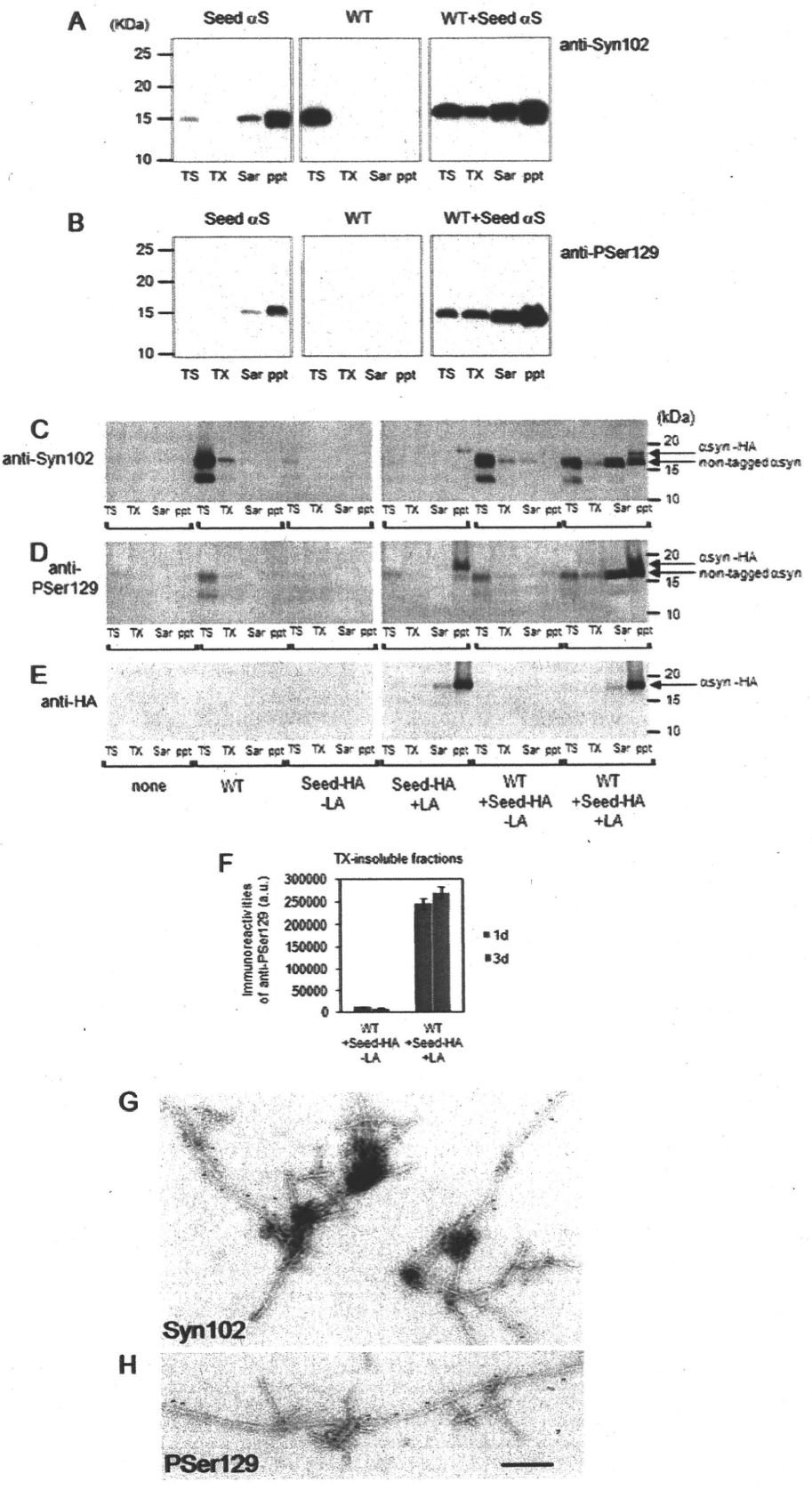

ble fractions compared with those in cells with wild-type α-syn expression and Seed αS (Fig. 5, *A* and *B*). In contrast, overexpression of Δ11 mutant α-syn, an assembly-incompetent mutant lacking residues 73–83, which have been shown to be essential for fibril formation of α-syn (24), elicited neither deposition nor phosphorylation of α-syn. We next introduced α-syn into SH-SY5Y cells expressing S129A mutant α-syn and observed slightly lower levels of Sarkosyl-insoluble α-syn compared with those in cells with wild-type α-syn expression and Seed αS. However, the frequency of inclusion bodies observed in seed-transduced cells expressing S129A was similar to that in seed-transfected cells expressing wild-type α-syn (data not shown), suggesting that phosphorylation at Ser^{129} is not required for the nucleation-dependent polymerization of α-syn within cells.

Nucleation-dependent Intracellular Polymerization of α-Syn Elicits Neurotoxicity and Cell Death—SH-SY5Y cells overexpressing α-syn started to show marked clumping suggestive of cellular degeneration and death by ~48 h after introduction of seeds (Fig. 6*B*). Quantitative analysis of cell death by a lactate dehydrogenase (LDH) release assay at 72 h after introduction of Seed αS showed that cells overexpressing wild-type, A30P, A53T, or S129A α-syn released ~30% of total LDH from total cell lysate, whereas only ~12% of LDH was released from cells expressing Δ11 mutant α-syn, which lacks polymerization ability. In control cells transfected with empty vector or pcDNA3-α-syn followed by treatment with Lipofectamine without seeds, only ~7% of LDH was released (Fig. 6*C*). These results suggest a close correlation between the seed-dependent aggregation of α-syn and cell death. However, the dying cells transfected with fibrillization-competent α-syn and seeds did not show typical morphological changes of apoptosis (*e.g.* nuclear fragmentation, positive TUNEL staining (supplemental Fig. S4*A*), or activation of caspase-3 (supplemental Fig. S4*B*)), suggesting that they did not undergo typical apoptotic cell death, despite a previous report that exposure to neuron-derived extracellular α-syn may cause apoptosis (25).

Impairment of Proteasome Activity in Cells with Intracellular Aggregates of α-Syn—Because α-syn is ubiquitinated in the brains of patients with α-synucleinopathies (26) and inhibition of ubiquitin-proteasome systems by aggregates of proteins with expanded polyglutamine tracts has been reported (27), we analyzed the ubiquitination state of cellular proteins in α-syn aggregate-forming cells and compared the pattern with that in cells treated with a proteasome inhibitor, MG132. A Sarkosyl-soluble fraction of seed-transduced cells expressing wild-type α-syn and harboring abundant inclusions showed increased levels of ubiquitin-positive staining, which was similar in pattern to that observed in cells treated with MG132 (Fig. 6*D*). Because this pattern suggested an impairment of the ubiquitin-proteasome system, we directly analyzed the proteasome activity of α-syn inclusion-forming cells using a specific fluorescent peptide substrate, benzyloxycarbonyl-Leu-Leu-Glu-7-amido-4-methylcoumarin, that emits fluorescence following proteasomal digestion and confirmed that proteasome activity was significantly reduced in these cells as well as in cells treated with 20 μM MG132 for 4 h (Fig. 6*E*). We further examined the suppression of proteasome activity using CL1, a short degron that has been reported to be an effective proteasome degradation signal (28) and whose fusion protein with green fluorescent protein (GFP-CL1) has been used as a reporter for inhibition of proteasomal activity by intracellular polyglutamine aggregates (27) and intracellular α-syn (19). To examine if intracellular α-syn inclusions affected proteasomal activity, SH-SY5Y cells were transfected with both wild-type α-syn and GFP-CL1, followed by the introduction of Seed αS. Fluorescent signals of GFP were scarcely detected in control cells transfected with GFP-CL1 alone (Fig. 6*F*, *none*) but were markedly increased upon treatment with proteasome inhibitor MG132 (Fig. 6*F*, *MG132*), confirming that GFP-CL1 was effectively degraded by proteasome. Strikingly elevated GFP signals were detected in cells forming α-syn inclusions (Fig. 6*F*, *WT + Seed αS*) compared with those in control cells (Fig. 6*F*, *none* or *WT*), and GFP-CL1 and deposits of phosphorylated α-syn were co-localized within these cells (*arrowheads*). These results strongly suggest that proteasome activity is impaired in cells harboring α-syn inclusions elicited by the introduction of Seed αS.

Small Molecular Inhibitors of Amyloid Filament Formation Protect against Cell Death Induced by Seed-dependent α-Syn Polymerization—We have previously shown that several classes of small molecular compounds inhibit amyloid filament formation of α-syn, Tau, and Aβ *in vitro* (17, 23). These observations prompted us to test whether these inhibitors exert a protective effect against death of SH-SY5Y cells mediated by the nucleation-dependent polymerization of α-syn. Fig. 7*A* shows the effects of three polyphenol compounds, exifone, gossypetin, and quercetin, and a rifamycin compound, rifampicin, added to the culture media at a final concentration of 20 or 60 μM. Remarkably, all of these compounds blocked cell death, with gossypetin being the most effective. Our previous *in vitro* studies elucidated that several polyphenols, including gossypetin and exifone, inhibit α-syn assembly and that SDS-stable, noncytotoxic soluble α-syn oligomers are formed in their presence (23), suggesting that such polyphenols may inhibit filament formation of α-syn by stabilizing soluble, prefibrillar intermediates. Gossypetin or exifone might suppress intracellular α-syn aggregate formation by stabilizing such soluble intermediates in cultured cells as well. Immunoblot analysis

FIGURE 3. **Immunoblot and immunoelectron microscopic analyses of intracellular α-syn aggregates in cultured cells.** *A* and *B*, immunoblot analysis of α-syn in cells treated with Seed αS alone (*Seed αS*), pcDNA3-α-syn alone (*WT*), or both WT and Seed αS (*WT + Seed αS*). Proteins were differentially extracted from the cells with Tris-HCl (*TS*), Triton X-100 (*TX*), and Sarkosyl (*Sar*), leaving the pellet (*ppt*). Blots were probed using anti-α-syn (Syn102) (*A*) and anti-$Ser(P)^{129}$ (*PSer129*) (*B*). *C–F*, immunoblot analysis of proteins differentially extracted from mock (none) or cells transfected with pcDNA3-α-syn (*WT*), cells transduced with Seed-HA with (*Seed-HA + LA*) or without LA treatment (*Seed-HA − LA*), and cells overexpressing α-syn treated with Seed-HA with (*WT + Seed-HA + LA*) or without LA treatment (*WT + Seed-HA − LA*). Immunoreactivity of phosphorylated α-syn in the Triton X-100-insoluble fraction was quantified using anti-$Ser(P)^{129}$, and the results are expressed as means ± S.E. ($n = 3$), as shown in *F*. a.u., arbitrary unit. *G* and *H*, immunoelectron microscopy of α-syn filaments extracted from transfected cells. SH-SY5Y cells were transfected with both pcDNA3-α-syn and Seed αS. Sarkosyl-insoluble fraction was prepared from the cells, and the filaments were immunolabeled with anti-Syn102 (*G*) or $Ser(P)^{129}$ (*H*) antibody. *Scale bar*, 200 nm. *1d* and *3d*, 1 and 3 days, respectively.

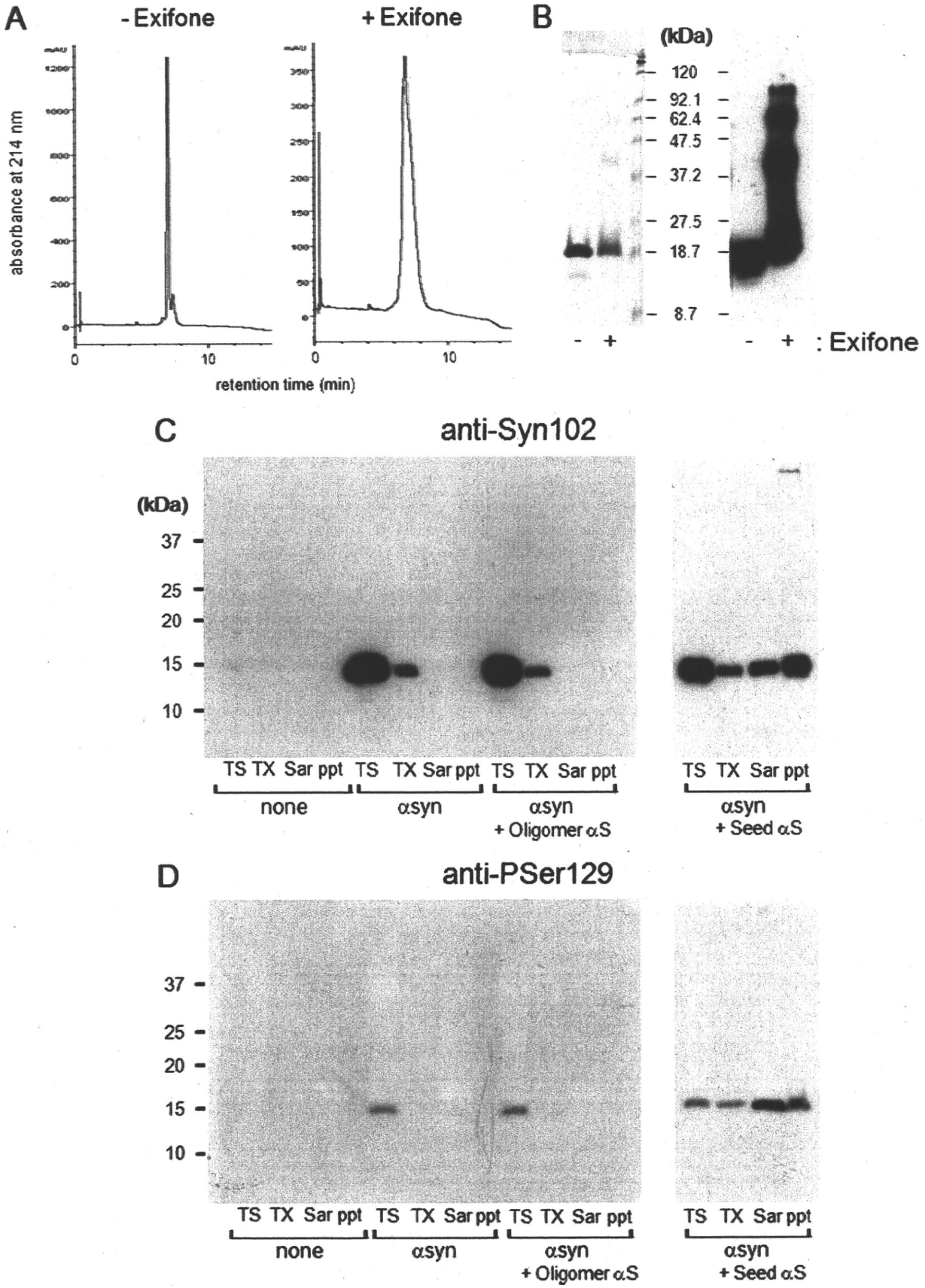

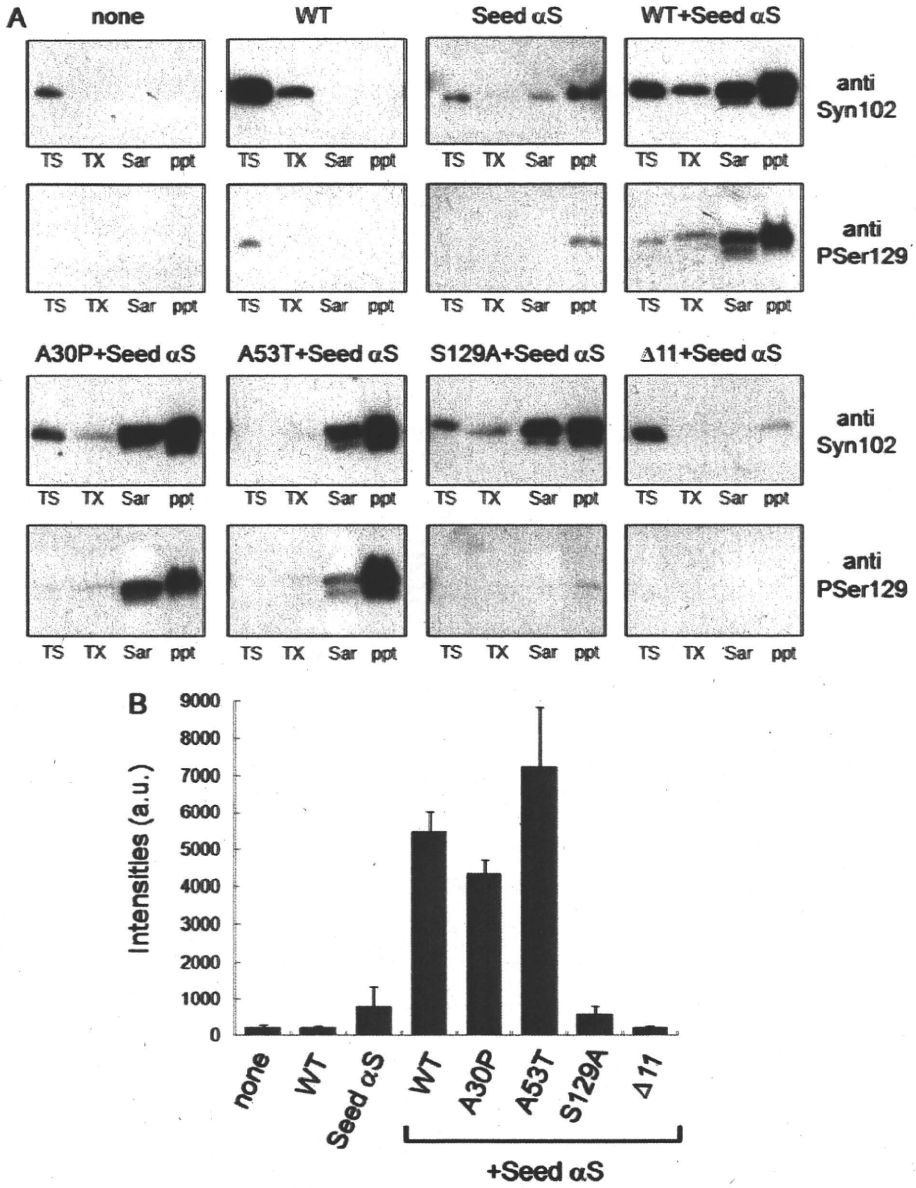

FIGURE 5. **Effects of α-syn mutations on intracellular deposition.** Immunoblot analysis of α-syn in cells transfected with pcDNA3-α-syn alone (*WT*), Seed αS alone (*Seed αS*), both WT and Seed αS (*WT + Seed αS*), and non-treated control cells (*none*). Cells overexpressing familial PD-linked A30P or A53T polymerization-deficient Δ11 mutant α-syn followed by transfection with Seed αS were also analyzed. Proteins were extracted differentially with Tris-HCl (*TS*), Triton-X (*TX*), and Sarkosyl (*Sar*), leaving the pellet (*ppt*), and immunoblotting was done with anti-Syn102 and Ser(P)^{129} (*PSer129*). The Ser(P)^{129}-immunoreactive bands detected in Sarkosyl-soluble and -insoluble fractions from each cell type shown in *A* were quantified (*B*). The results are expressed as means +S.E. (*error bars*) ($n = 3$). a.u., arbitrary unit.

revealed that the levels of Sarkosyl-insoluble α-syn in cells transfected with both α-syn and seeds were reduced by treatment with exifone or gossypetin compared with those in untreated cells (Fig. 7*B*), supporting the notion that these compounds entered the cytoplasm and blocked cell death by suppressing the seed-dependent polymerization of α-syn.

Cellular Models for Nucleation-dependent Polymerization of Tau—Beside α-syn, Tau is another major pathogenic protein that is deposited in degenerating neurons or glial cells in various neurodegenerative diseases, and aggregation of distinct Tau isoforms has been found in different diseases (*i.e.* deposition of three-repeat Tau isoforms in Pick's disease, four-repeat Tau isoforms in progressive supranuclear palsy and corticobasal degeneration, and both three- and four-repeat Tau isoforms in AD). It is unknown why distinct Tau isoforms deposit in different diseases. Thus, we also tried to establish a cellular model of intracellular Tau aggregate formation by transduction of Tau fibril seeds into cultured cells. First, we confirmed that expression of 3R1N or 4R1N by itself induced phosphorylation of Ser^{396}, but no aggregated form was detected in detergent-insoluble fractions (Fig. 8 and **supplemental Fig. S5**). Next, we tested whether introduced Tau 4R1N or 3R1N fibril seed (Seed 4R1N or 3R1N, respectively) is detectable by immunoblot analysis using anti-T46, anti-HT7, or anti-Ser(P)^{396} antibody. However, we could not detect any band in Triton X-100-insoluble fractions of cells treated with Seed Tau 4R1N or 3R1N in the presence of LA with any of these antibodies (data not shown). It seems likely that the efficiency of introduction of Tau 4R1N and 3R1N fibrils by LA treatment is very low, as compared with that of Seed αS. Then we checked whether treatment with recombinant Tau fibrils causes intracellular Tau aggregate formation in an LA-dependent manner. As shown in **supplemental Fig. S5**, LA treatment itself did not cause intracellular Tau deposition in cells expressing Tau 4R1N without

FIGURE 4. **α-Syn oligomers were not introduced into cultured cells.** *A* and *B*, α-Syn oligomers were prepared as described under "Experimental Procedures." Oligomeric α-syn protein incubated with (47.8 μg of protein) or without exifone (30 μg of protein) was analyzed by reversed-phase HPLC (Aquapore RP-300 column) (*A*). These samples (0.2 μg of protein of each) were also analyzed by SDS-PAGE and immunoblotted with anti-Syn102 (*B*). *C* and *D*, cells were transfected with empty plasmid (*none*) or pcDNA3-αsyn (*αsyn*) and then treated with or without α-syn oligomer (*Oligomer αS, 5 μg*) or fibrils (*Seed αS, 2 μg*). After incubation for 3 days, cells were harvested, and immunoblot analyses were performed. Proteins differentially extracted from the cells with Tris-HCl (*TS*), Triton X-100 (*TX*), Sarkosyl (*Sar*), and the pellet (ppt) were probed using anti-Syn102 (*C*) and anti-Ser(P)^{129} (*PSer129*) (*D*).

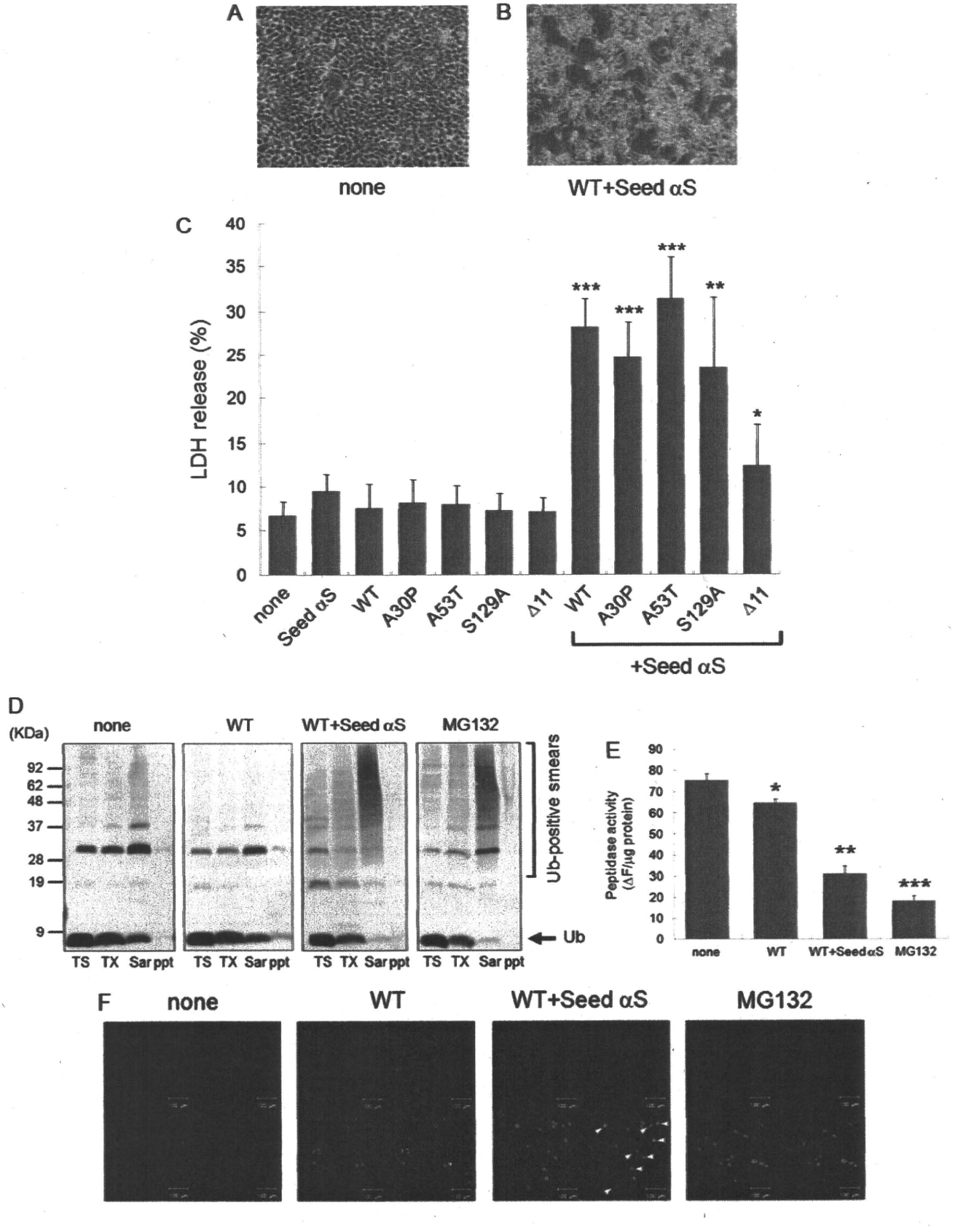

Seed 4R1N. Recombinant Tau 4R1N monomer in the presence of LA did not elicit the formation of intracellular Tau aggregates in these cells. On the other hand, when Seed 4R1N was added to cells expressing Tau 4R1N with LA, aggregated and phosphorylated Tau was detected in Sarkosyl-insoluble fractions by immunoblot analyses of these cell lysates using anti-HT7 or anti-Ser(P)^{396} antibody (**supplemental Fig. S5** and Fig. 8). In the case of intracellular Tau 3R1N aggregate formation, the results were similar to those in the experiments using Tau 4R1N described above (data not shown).

Intracellular aggregated four- or three-repeat Tau was also found to be detected with not only anti-Ser(P)^{396} but also anti-AT100 antibody in the Sarkosyl-insoluble fraction (Fig. 8, *B* and *C*). Phosphorylated and deposited Tau was not found in the Triton X-100-insoluble fraction of Tau-expressing cells without Tau seed treatment or mock plasmid-expressing cells treated with Tau seed. In accordance with findings described earlier in this paper, these results suggested that soluble four- or three-repeat Tau expressed from the plasmid was accumulated into intracellular inclusions in the presence of small amounts of Seed 4R1N or 3R1N.

We also found that hyperphosphorylated and aggregated Tau was not detected in three-repeat Tau-expressing cells treated with Seed 4R1N (Fig. 8, *B* and *C*). On the other hand, the aggregated form of three-repeat Tau was detected in Triton X-100-insoluble fractions of three-repeat Tau-expressing cells treated with Seed 3R1N, and hyperphosphorylation at Ser^{396} and Ser^{212}/Thr^{214} was observed in fractionated samples of these cells, whereas no such bands were detected in four-repeat Tau-expressing cells treated with Seed 3R1N (Fig. 8, *B* and *C*). These results clearly showed that four-repeat Tau fibrils can be seeds for polymerization of four-repeat Tau, and three-repeat Tau fibrils can be seeds for polymerization of three-repeat Tau. Tau does not polymerize (cross-seed) in the presence of seeds of a different isoform. Similarly, no Tau aggregation was detected in Tau-expressing cells treated with α-syn fibril seeds (**supplemental Fig. S3**, *C* and *D*), and no α-syn aggregation was detected in α-syn-expressing cells transduced with Tau fibril seeds (data not shown). Furthermore, we observed anti-AT100 and anti-Ser(P)^{396}-positive Tau 4R1N or 3R1N filaments of ~15-nm width by negative stain electron microscopic analyses of Sarkosyl-insoluble fractions of cells transfected with both Tau plasmid and the seeds (Fig. 9, *A–D*).

Confocal microscopic analyses also showed that GFP-tagged Tau 4R1N (GFP-Tau 4R1N) is aggregated into round inclusions in the presence of Seed 4R1N together with LA (Fig. 8*E*). No inclusion-like structures were found in cells expressing GFP-Tau 4R1N (Fig. 8*D*) or in cells expressing GFP-Tau 4R1N after treatment with Seed 3R1N (data not shown). The ratio of the round aggregates to all GFP-positive transfectants was calculated to be 5.8% ± 0.8602 ($p = 0.0002$ by Student's t test against the value of cells expressing GFP-4R1N, $n = 5$). Significant cell death was not observed in cells containing intracellular 3R1N or 4R1N aggregates (data not shown). These results strongly suggest that proteins assemble easily into amyloid fibrils in the presence of amyloid seeds derived from the same protein but not a different protein.

DISCUSSION

Nucleation-dependent protein polymerization occurs in many well characterized physiological processes (*e.g.* microtubule assembly and actin polymerization). It is also the mechanism of amyloid fibril formation in various pathological conditions and has been confirmed to occur *in vitro* for a wide variety of extracellular amyloids, such as Aβ peptides and prion proteins (12, 13) as well as intracellular proteins, such as α-syn and Tau (29, 30, 42). Both extra- and intracellular amyloids have been well studied *in vitro*, but much less is known about the mechanisms of assembly *in vivo*. Here we report a simple and effective method to introduce polymerization seeds into cells using Lipofectamine, a widely used transfection reagent. This method enabled us to evaluate the nucleation-dependent polymerization of α-synuclein and to establish a cellular model of the neurodegeneration seen in Parkinson disease.

Lipofectamine is a reagent widely used for the transfection of DNA into eukaryotic cells through the formation of liposomes of polycationic and neutral lipids in water, based on the principle of cell fusion. Various methods, including microinjection, the calcium phosphate method, the DEAE-dextran method, electroporation, and viral transfer, have been employed to introduce substances that are not normally incorporated into eukaryotic cells under physiological conditions. Microinjection is versatile but is not efficient in experiments involving large numbers of cells, and the traumatic damage to cells hampers evaluation of cytotoxic effects. Here, we have successfully employed lipofection to introduce protein aggregates as seeds

FIGURE 6. **Cell death caused by formation of intracellular α-syn inclusions.** *A* and *B*, phase-contrast microscopy of the control cells (*A*) and cells transfected with both pcDNA3-α-syn and Seed αS (*B*) 3 days after treatment with Seed αS (20× objective). *C*, the extent of cell death of transfected cells was quantified using an LDH release assay. Cells transfected with α-syn plasmid alone (WT, A30P, A53T, S129A, or Δ11) or with both wild-type or several mutants and Seed αS were incubated, and the cell death assay was performed 3 days thereafter. The results are expressed as means +S.E. (*error bars*) ($n = 5$). *, not significant; **, $p < 0.01$; ***, $p < 0.0005$ by Student's t test against the value of Seed αS. *D–F*, impairment of proteasome activity caused by intracellular aggregates of α-syn. *D*, immunoblot analysis of proteins sequentially extracted from non-treated cells (*none*) and cells transfected with wild-type α-syn plasmid alone (*WT*) or with both pcDNA3-α-syn and Seed αS (*WT + Seed αS*) and cells treated with 1 μM MG132 for 16 h (MG132) using anti-ubiquitin antibody. An *arrow* indicates monomeric ubiquitin. Polyubiquitinated proteins, reflecting impairment of the proteasome activity, are observed in the Sarkosyl-soluble fraction. *TS*, Tris-soluble; *TX*, 1% Triton X-100-soluble; *Sar*, 1% Sarkosyl-soluble; *ppt*, Sarkosyl-insoluble and SDS-soluble. *E*, peptide hydrolysis activity of proteasome. Cytosol fractions of non-treated control cells (*none*), cells transfected with wild-type α-syn plasmid alone (*WT*) or with WT and Seed αS (*WT + Seed αS*), and cells treated with 20 μM MG132 for 4 h (*MG132*) were prepared and assayed using benzyloxycarbonyl-Leu-Leu-Glu-7-amido-4-methylcoumarin as a substrate. The results are expressed as means +S.E. ($n = 3$). *, $p < 0.05$; **, $p < 0.01$; ***, $p < 0.0005$ by Student's t test against the value of none. *F*, proteasome activity in cells having intracellular aggregates of α-syn. SH-SY5Y cells transfected with both GFP-CL1 and WT were treated with Seed αS for 2 days, fixed, and stained with anti-Ser(P)^{129}. In the staining of cells transfected with wild-type α-syn plasmid alone (*WT*), anti-Syn102 was used. As a control, untreated or MG132-treated cells were also stained and analyzed. In untreated control cells, the fluorescence of GFP was poorly detected because GFP-CL1 could be degraded by proteasome in cells. In cells treated with MG132, fluorescence was markedly increased as compared with that in untreated cells because of the inhibition of proteasome activity by MG132. Co-localized images (*arrowheads*) with both increased intensities of GFP (*green*) and the fluorescence of anti-Ser(P)^{129} (*red*) were detected in cells transfected with both WT and Seed αS (*WT + Seed αS*), indicating that the proteasome activity in these cells was inhibited.

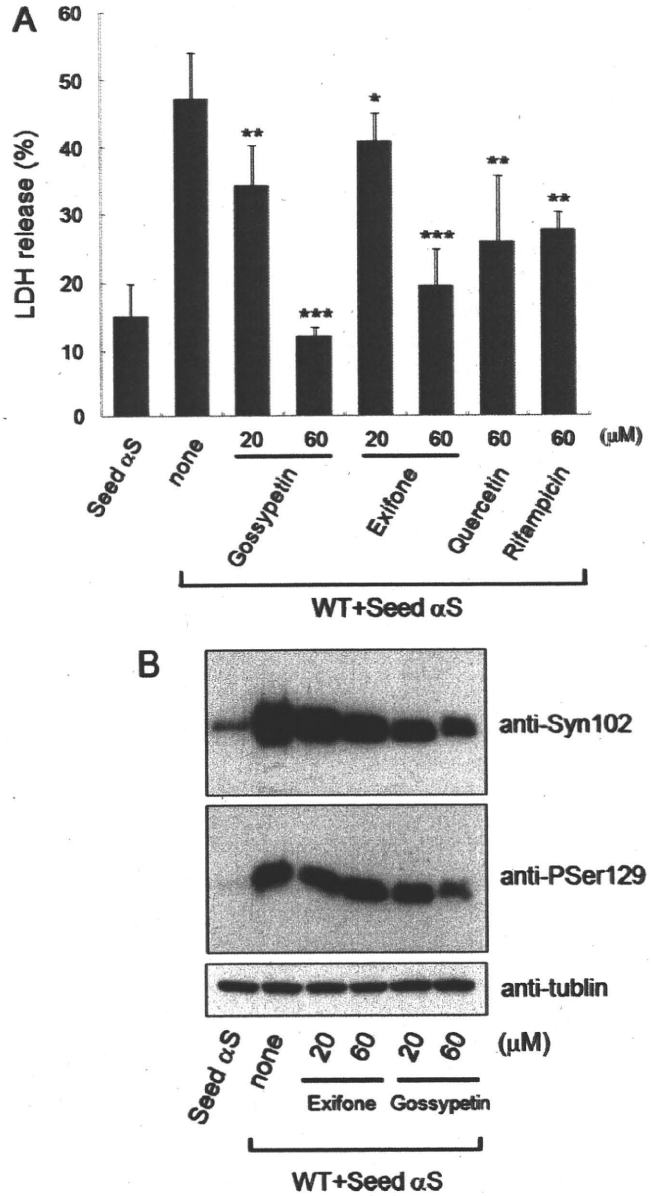

FIGURE 7. **Small molecular inhibitors of amyloid filament formation protect against cell death caused by intracellular α-syn aggregates.** *A*, the cell death of cells transfected with Seed αS and with both α-syn plasmid (*WT*) and Seed αS in the presence or absence of 20 or 60 μM gossypetin, 20 or 60 μM exifone, 60 μM quercetin, or 60 μM rifampicin was quantified by LDH release assay. The results are expressed as means ± S.E. (*error bars*) ($n = 4$). *, not significant; **, $p < 0.05$; ***, $p < 0.0005$ by Student's *t* test against the value of none. *B*, immunoblot analyses of the Sarkosyl-insoluble fraction prepared from cells transfected with Seed αS and with both WT and Seed αS in the absence or presence of exifone or gossypetin, with anti-Syn102 and anti-Ser(P)^{129} (*PSer129*) antibodies. Doubly transfected cells were treated with 20 or 60 μM exifone or gossypetin 2 h after transfection of Seed αS and cultured for 3 days in the presence of polyphenols. Tubulin-α loading controls are also shown.

for amyloid fibril formation (patent pending for the United States (12/086124), the European Union (06834541.2), and Japan (2007-549210)). The reason why Lipofectamine could specifically incorporate Seed αS but not soluble α-syn into cells is unknown. However, one possibility is that aggregated α-syn with an ordered filamentous structure was preferentially bound to Lipofectamine and formed a complex that could be more effectively transported into cells compared with soluble α-syn, which has a random coil structure. In line with this idea, it has been reported that yeast prion fibrils can be introduced into yeast cells (31). Recently, Luk *et al.* (32) have also reported that α-syn monomers and fibrils but not oligomers were introduced into cells by Bioporter, a cationic-liposomal protein transduction reagent.

We confirmed the incorporation of insoluble α-syn seeds into cells by detecting phosphorylation of α-syn, as has been seen in intracellular aggregates of α-syn in various neurodegenerative conditions referred to as synucleinopathies. This suggests that Seed αS introduced into cells is a good target for phosphorylation at Ser^{129}. In contrast to our results, a recent report suggested that α-syn fibrils were not phosphorylated after internalization (32). It is possible that this specific phosphorylation represents an active attempt by cells to maintain the intracellular milieu by sequestering protein species that are harmful to cells. Notably, the phosphorylation of α-syn was dramatically increased when Seed αS was introduced into cells overexpressing soluble α-syn (Fig. 3 and **supplemental Figs. S1*D* and S2**). The possibility therefore arises that widespread propagation of hyperphosphorylation of α-syn throughout the cytoplasm reflects the activation of a certain kinase(s) associated with conversion of soluble α-syn into the fibrillar form in the presence of Seed αS. However, further investigation is needed to elucidate the importance of phosphorylation for protein aggregation.

The significance of intracellular and extracellular protein aggregates in neurodegeneration is still a matter of debate. The present results clearly show that nucleation-dependent polymerization of amyloid-like proteins is closely related to neuronal degeneration leading to cell death. According to the seeding theory, amyloid fibrils grow rapidly, without a time lag, when seeds are exposed to an amount of amyloidogenic soluble protein that exceeds the critical concentration. Our experiments with seed-transfected SH-SY5Y cells overexpressing α-syn clearly demonstrated that this is the case in the intracellular environment. We have unequivocally demonstrated that nucleation-dependent polymerization of amyloid-like fibrils can occur inside cells, and the intracellular filament formation elicits a variety of cellular reactions, including hyperphosphorylation and compromise of the ubiquitin proteasome system. We also showed that α-syn oligomers were not introduced into cells by LA and did not function as seeds for α-syn aggregate formation in cultured cells. It has been speculated that protein fibrils, not oligomers, are spread or transmitted in recently reported *in vivo* models (25, 33).

Our study also revealed that intracellular protein aggregation is highly dependent on the species of protein fibril seeds. This important finding may explain why only certain Tau isoforms are deposited in several tauopathies, including Pick disease, progressive supranuclear palsy, and corticobasal degeneration. In this study, α-syn fibrils were shown to be unable to seed intracellular Tau aggregation, which is consistent with neuropathological reports that deposited α-syn is not markedly co-localized with Tau aggregates. Our observations strongly support a seed-dependent mechanism for the formation of the intracellular protein aggregates.

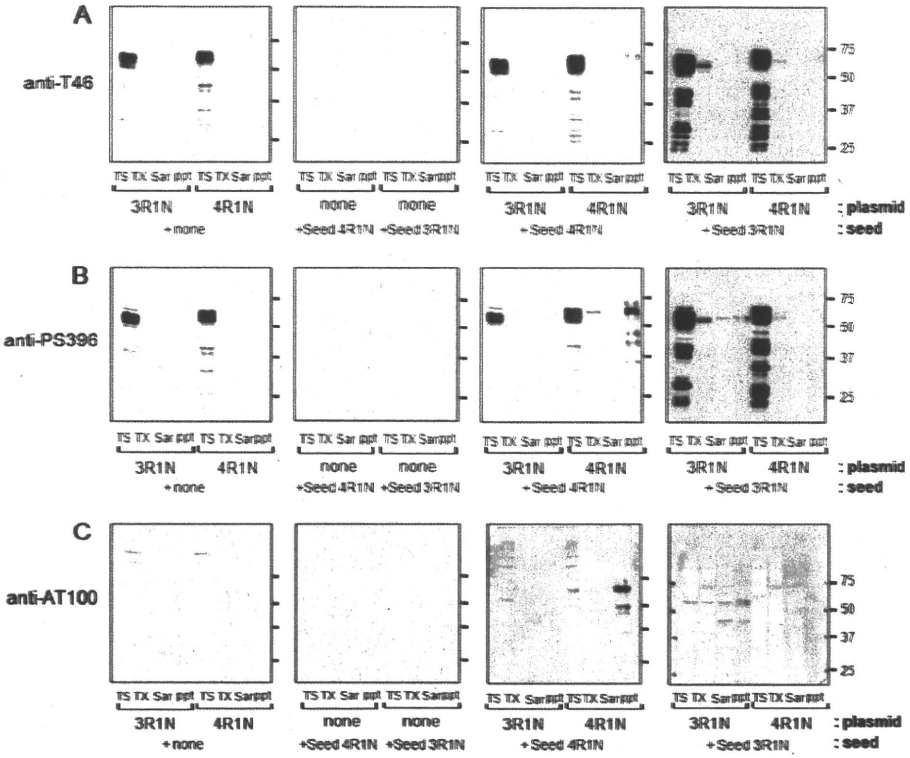

FIGURE 8. **Immunoblot analyses of intracellular Tau aggregates.** *A–C*, immunoblot analysis of Tau in cells treated with Tau fibrils alone (Seed 3R1N or Seed 4R1N), pcDNA3-Tau alone (3R1N or 4R1N), or both Seed Tau and pcDNA3-Tau. Tau proteins differentially extracted from the cells with Tris-HCl (*TS*), Triton X-100 (*TX*) and Sarkosyl (*Sar*), and the pellet (*ppt*) were probed with anti-T46 (*A*), anti-Ser(P)^{396} (*PS396*) (*B*), and anti-AT100 (*C*).

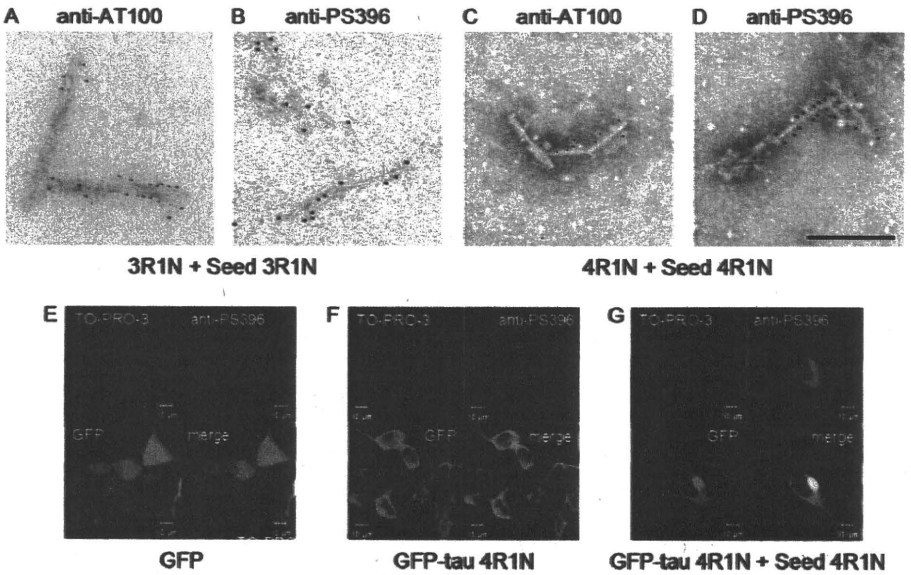

FIGURE 9. **Cellular models for intracellular Tau aggregation.** *A–D*, immunoelectron microscopy of Tau filaments extracted from transfected cells. SH-SY5Y cells were transfected with both pcDNA3-Tau 3R1N and Seed 3R1N (*A* and *B*) or pcDNA3-Tau 4R1N and Seed 4R1N (*C* and *D*). The Sarkosyl-insoluble fraction was prepared from the cells, and the filaments were immunolabeled with anti-AT100 (*A* and *C*) or anti-Ser(P)^{396} (*PS396*) (*B* and *D*) antibody. *Scale bar*, 200 nm. *E–G*, confocal laser microscopic analyses of SH-SY5Y cells transfected with pEGFP empty vector (*E*), pEGFP-Tau 4R1N (*F*), and cells transfected with both pEGFP-Tau 4R1N and Seed 4R1N (*G*), immunostained with anti-Ser(P)^{396} (*red*), and counterstained with TO-PRO-3 (*blue*). *Scale bars*, 10 μm.

Importantly, we showed that seed α-syn or Tau, an insoluble aggregate prepared from α-syn or Tau filaments, is effectively incorporated into cells by lipofection. This, in turn, suggests that high molecular weight protein aggregates or amyloid seeds shed from one cell may easily be propagated to others (*e.g.* neurons or glial cells) under pathological conditions (*e.g.* alteration in membrane permeability due to aging or virus infection, impairment of membrane function as a result of physical interaction with extracellular amyloid deposits, or abnormal membrane depolarization) that favor intracellular deposition of protein fibrils.

It remains to be clarified whether the incorporation of amyloid seeds into neurons or glial cells, as shown in this study, also occurs *in vivo*. However, some observations in AD or in transgenic animals support this possibility; apolipoprotein E (apoE) is involved in lipoprotein particle uptake mediated by cell surface receptors, and the E4 allele is the strongest genetic risk factor for AD. The apoE polypeptide has also been shown to bind Aβ (34), Tau (35), and the non-Aβ component of Alzheimer disease region of α-syn (36) and to be localized in amyloid plaques and neurofibrillary tangles in AD and prion plaques (37) in Creutzfeldt-Jakob disease. ApoE and low density lipoprotein receptor-related protein facilitate intraneuronal Aβ42 accumulation in transgenic mice (38). Furthermore, activation of both endocytic uptake and recycling of these proteins at a preclinical stage has been reported in sporadic AD and Down syndrome (39). Thus, it is strongly suggested that extracellular amyloid may be taken up into neurons by apoE and lipoprotein receptor-related protein-mediated endocytosis. Therefore, intracellular amyloid seeds composed of α-syn or Tau may also be incorporated into neurons by similar mechanisms when these seeds are released to the extracellular space after neuronal death.

It is well established that Tau protein starts to accumulate in the entorhinal region and spreads to the neocortices, closely correlating with the progression of AD (40). Similarly, accumulation of phosphorylated α-syn has been shown to start in vulnerable regions (*i.e.* limbic cortices) and to spread to the neocortices in PD or DLB. However, the mechanism of propagation of abnormal